

# Estimating the Electric Fields Driving Lightning Dart Leader Development with BIMAP-3D Observations

Daniel P. Jensen<sup>1,2</sup>, Xuan-Min Shao<sup>1</sup>, Richard G. Sonnenfeld<sup>2</sup>,  
and Caitano L. da Silva<sup>2</sup>

<sup>1</sup>Electromagnetic Sciences & Cognitive Space Applications, Los Alamos National Laboratory,  
Los Alamos, NM, USA

<sup>2</sup>Langmuir Laboratory for Atmospheric Research, New Mexico Institute of Mining and Technology,  
Socorro, NM, USA

## Key Points:

- We estimate cloud ambient electric fields by combining 3D mapping and electric field change observations with an equipotential leader model
- Our results are consistent with the hypothesis that dart leader speed is proportional to the leader tip electric field
- The modeled tip fields also explain why dart leaders typically follow previous channels and appear very narrow compared to step leaders

---

Corresponding author: Daniel Jensen, [dpjensen@lanl.gov](mailto:dpjensen@lanl.gov)

**Abstract**

In this paper, a numerical dart leader model has been implemented to understand the leader's development and the corresponding electric field changes observed by the 3D Broadband Mapping And Polarization (BIMAP-3D) system. The model assumes the extending leader channel is equipotential and has a linear charge distribution induced by an ambient electric field. The charge distribution induced by the ambient field can be used to model the electric field change at the ground. We then find the ambient electric field which best fits the field change measurements at the two BIMAP stations. The estimated ambient electric field decreases in the direction of dart leader propagation. Our observations and modeling results are consistent with our earlier hypothesis that dart leader speed is proportional to the electric field at the leader tip. The model also supports our earlier analysis that leader speed variations near branch junctions were due to previous charge deposits near the junctions. The modeled tip electric field is generally lower than the breakdown field unless the pre-dart-leader channel has a significant temperature of  $\sim 3000$  K. This is consistent with the fact that dart leaders typically do not form new branches into the virgin air. Furthermore, the tip field is generally close to the negative streamer stability field at ambient temperatures, explaining the nature of the narrow and well-defined channel structure. In addition to the charge distribution and the ambient and tip electric field, the development of the channel potential and current distribution are also presented.

**Plain Language Summary**

A dart leader is a discharge process that occurs at the later stage of a lightning flash. It retraces the path established by earlier discharges and propagates at a high speeds of 1%-10% the speed of light. Recently we developed a system called BIMAP-3D that can map lightning radio sources in 3D with high time resolution. We also measured the electric field at the ground caused by lightning discharges. In this paper we modeled a 3D mapped dart leader as a perfectly conducting wire. A conducting wire placed in an external electric field disturbs the field around it. We used our wire dart leader model to find an electric field in the cloud so that the modeled disturbance matched the electric fields we measured at the ground. The estimated cloud field decreases in the direction of dart leader propagation. Our model suggests that the speed of a dart leader is closely related to electric field at the dart leader tip. The modeled electric field at the dart leader tip is also too low to form a new discharge path through the air, explaining why they follow previously established paths.

**1 Introduction**

In Jensen et al. (2023b) we analyzed 14 in-cloud dart leaders (also called K-leaders or recoil leaders) with 3D Broadband Interferometric Mapping And Polarization (BIMAP-3D) observations. The dart leaders often exhibited an overall initial acceleration and a gradual deceleration, and some rapid speed variations as the leaders passed branch junctions in the flash structure. We proposed that the dart leader speed was proportional to the electric field strength at the leader tip when the leader is considered an equipotential channel growing through an ambient electric field. Based on the overall speed trend, it was inferred that the ambient electric field decreases in the direction of the leader propagation. We also used a simple two-point dipole charge model to estimate the development of the charge distribution along the leader channel based on the field change measured by two fast electric field change antennas. This paper expands on the work of Jensen et al. (2023b) by numerically modeling the development of equipotential dart leader channels constrained by our BIMAP-3D and fast antenna observations.

The leader model used in this study was first suggested by Kasemir (1960), who applied the basic concepts of electrostatics to approximate conductive lightning chan-

66 nels as equipotential and growing in an electric field, with qualitative descriptions of the  
 67 induced charge distribution. Mazur and Ruhnke (1993, 1998) expanded upon Kasemir’s  
 68 initial work with numerical modeling of equipotential lightning channels. The model of  
 69 Kasemir (1960) has historically been referred to as the bidirectional leader model, we will  
 70 instead refer to it as the equipotential leader model, since the equipotential assumption  
 71 is the most significant difference between this model and other non-physics-based leader  
 72 models. A number of studies have used measured field changes to model simple charge  
 73 configurations along leader channels without considering leader conductivity (Cai et al.,  
 74 2022; Chen et al., 2013; Gao et al., 2020; Jensen et al., 2023b; Karunarathne et al., 2015;  
 75 Lu et al., 2011). By contrast relatively few studies have attempted to compare the equipo-  
 76 tential model to observed electric field changes associated with lightning (Mazur & Ruhnke,  
 77 1993; Pasko, 2014; da Silva & Pasko, 2015), and these studies have been somewhat lim-  
 78 ited by lack of knowledge of the extent or location of the leader channel.

79 The BIMAP-3D system has the capability to map out very high frequency (VHF)  
 80 radio sources along lightning channels in 3D over time (Shao et al., 2023), and simul-  
 81 taneously measures the electric field changes with a fast antenna at each of the two BIMAP  
 82 stations. If we assume the active and continuous dart leader channel sections with re-  
 83 cent VHF activity are at equipotential, and choose some reasonable channel radius, the  
 84 only remaining unknown in the model is the cloud electric field distribution along the  
 85 channel. The cloud electric field can then be estimated through standard non-linear in-  
 86 verse problem techniques as described in Section 3.

87 This approach to indirectly measuring the ambient electric field is similar in con-  
 88 cept to the work reported by Cummer (2020), but our use of time resolved leader lengths  
 89 and field changes allows the estimated ambient field along the leader channel to be spa-  
 90 tially resolved. This additional information leads to a number of insights on the phys-  
 91 ical conditions of the developing channel.

92 As a note on terminology, in our previous papers (Jensen et al., 2021, 2023b) we  
 93 have discussed the use of the terms “K-leader”, “dart leader”, and “recoil leader” to re-  
 94 fer to what is fundamentally the same phenomenon. Following some recent discussion  
 95 and consensus within at least part of the lightning community (Hare et al., 2023b, 2024;  
 96 da Silva et al., 2023) we now choose to use the term dart leader exclusively to refer to  
 97 this phenomenon, as we previously suggested in Jensen et al. (2021). To avoid confusion  
 98 about whether a dart leader is followed by a return stroke we suggest that dart leaders  
 99 may be further classified as in-cloud (IC) dart leaders or cloud-to-ground (CG) dart lead-  
 100 ers whenever the distinction is relevant, as we suggested in Jensen et al. (2021).

101 Following this terminology convention, in this paper we apply the equipotential model  
 102 to IC dart leaders to understand the electric fields and other conditions that drive the  
 103 leader’s development. This work builds on recently reported observations of dart lead-  
 104 ers (Jensen et al., 2023b), and serves as a more rigorous test of some of our hypotheses  
 105 on the dart leader propagation physics. When applying the methodology discussed in  
 106 Section 3 the model results are consistent with our hypothesis that dart leader speed is  
 107 proportional to the leader tip electric field, as we first suggested in Jensen et al. (2021).  
 108 We demonstrate that an ambient field which starts relatively high and decreases along  
 109 the channel results in a tip field that matches the observed speed trends of initial accel-  
 110 eration and gradual deceleration. We also confirm that the branch junction speed vari-  
 111 ations can be explained by charge deposits near the primary channel. Our results also  
 112 provide possible explanations to some other observed dart leader properties, such as their  
 113 well-defined and narrow channel width in VHF and the fact that they typically do not  
 114 exit the pre-conditioned channel structure to propagate through virgin air.

## 2 Instrumentation

In this paper we make use of lightning observations from the BIMAP-3D system (Shao et al., 2023) that has been deployed at Los Alamos National Laboratory (LANL) since 2021. It consists of two stations, each with four VHF antennas arranged in a Y configuration. The two stations are 11.5 km apart. Lightning data from each station is first processed separately to form a 2D lightning map, and then is combined and reprocessed to produce a 3D lightning map. Based on observations of dart leader channel widths the random uncertainty of BIMAP-3D can be better than 10 m in easting, northing, and altitude in ideal conditions (Shao et al., 2023). Systematic biases in the absolute location have not been evaluated, but the 3D results produced by the triangulation and DTOA location techniques typically differ by less than 30-50 m, and this gives an estimate of the absolute location error. For lightning channels several kilometers away a location bias of 50 m is negligible for this study.

BIMAP-3D also has a fast electric field change antenna, or fast antenna (FA) at each station. The fast antenna at station 1 (FA01) has a highpass time constant of 1 ms, and the fast antenna at station 2 (FA02) has a time constant of 0.2 ms. For a first order highpass filter the low frequency content can be reliably recovered by de-drooping (deconvolution) (Födisch et al., 2016; Sonnenfeld et al., 2006) as long as the low frequency signal is sufficiently above the noise level, the direct current (DC) offset or “zero-level” of the signal is reliably known, and the signal does not saturate. For both FA01 and FA02 the low frequency content can be recovered down to the 60 Hz noise from nearby power infrastructure. There is no explicit lowpass filter in the fast antennas, but above 20 MHz there is essentially no signal. In this study we are interested in the electrostatic field change associated with the dart leaders, so we digitally lowpass the signals at 25 kHz. The field change signals we are analyzing are thus more in the slow antenna regime. We also de-droop the field change for each dart leader separately, making use of the fact that there is essentially no field change in the interval between dart leaders for this flash.

In Jensen et al. (2023b) we found a relative calibration between FA01 and FA02 by comparing peak amplitudes for distant return strokes. This relative calibration was sufficient for qualitative modeling analysis. For quantitative modeling in this paper, we need an absolute calibration for each fast antenna. To achieve this we used 48 hours of National Lightning Detection Network (NLDN) peak current data for strikes within 100 km of our stations that were captured by either of our stations. We restricted the NLDN data set to strikes that were at least 15 km away from both stations, and with reported peak currents between 0 kA and -50 kA. With these restrictions we found 263 strikes for FA01 and 87 strikes for FA02. To compare NLDN peak currents to our field change measurements we used the empirical relation of Equation 4 in Nag et al. (2014) (first reported by Rakov et al. (1992) based on results from Willett et al. (1989)). Based on this equation we derived calibration factors for our fast antennas based on each NLDN strike, with units of  $\left[\frac{V}{m}\right]$  per digital count. After finding the calibration factor for each match between the NLDN and our fast antennas, and removing any obvious outliers, we found the average calibration factor for each station. The calibration factors were  $4 \pm 2$  mV/(m-count) for FA01 and  $2 \pm 1$  mV/(m-count) for FA03. In each case the  $1\sigma$  uncertainties are about 50% of the calibration value. This is a significant source of uncertainty for all the quantities calculated in this paper.

## 3 Methods

### 3.1 The Equipotential Leader Model

Following the approach of Mazur and Ruhnke (1998), we consider a lightning leader as a long cylinder with length  $L$  and effective capacitive radius  $r_C$ . If the cylindrical channel is placed in an ambient potential distribution  $\Phi_{amb}(s)$  and a linear charge distribu-

165 tion  $\lambda(s)$  is placed along the channel, then the new potential along the channel  $\Phi(s)$  will  
 166 be given by:

$$\Phi(s) = \Phi_{amb}(s) + \frac{1}{4\pi\epsilon_0} \int_{s_a}^{s_b} \frac{\lambda(s') ds'}{\sqrt{(s-s')^2 + r_C^2}} \quad (1)$$

167 where  $s$  is the coordinate along the length of the channel.  $s_a$  and  $s_b$  are the ends of the  
 168 channel.

169 For an assumed equipotential channel we have  $\Phi(s) = \Phi_{cha} = const.$  for  $s_a \leq$   
 170  $s \leq s_b$ . We further assume that the leader has no net charge, since the transfer of charge  
 171 between the leader and the cloud should be negligible at dart leader time scales. Under  
 172 these assumptions the channel potential must be given by the average value (Mazur et  
 173 al., 1995):

$$\Phi_{cha} = \frac{1}{s_b - s_a} \int_{s_a}^{s_b} \Phi_{amb}(s) ds \quad (2)$$

174 We then wish to find the charge distribution  $\lambda(s)$  which satisfies this condition. To  
 175 evaluate this numerically with the method of moments technique we discretize the leader  
 176 channel into  $N$  segments of length  $\Delta s$ , where each segment has a uniform charge den-  
 177 sity. We then linearize Equation 1 as (da Silva & Pasko, 2015):

$$[\Phi_i] = [\Phi_{amb,i}] + [K_{i,j}] [\lambda_j] \quad (3)$$

178 where  $\Phi_i$  is the net potential at  $s_i$ ,  $\Phi_{amb,i}$  is the ambient potential at  $s_i$ , and  $[K_{i,j}] [\lambda_j]$   
 179 gives the approximate potential at  $s_i$  due to the linear charge density  $\lambda_j$  at every loca-  
 180 tion  $s_j$  along the channel.  $\Phi_i$ ,  $\Phi_{amb,i}$ , and  $\lambda_j$  are the elements of column matrices of size  
 181  $N \times 1$ , and  $K_{i,j}$  are the elements of an  $N \times N$  matrix defined as

$$K_{i,j} = \frac{1}{4\pi\epsilon_0} \int_{s_j - \Delta s/2}^{s_j + \Delta s/2} \frac{ds'}{\sqrt{(s_i - s')^2 + r_C^2}} \quad (4)$$

182 where  $K_{i,j}$  has units of meters per Farad.

183 The discretized charge distribution can then be obtained as:

$$[\lambda_j] = [K_{i,j}]^{-1} [\Phi_{amb,i} - \Phi_{cha}] \quad (5)$$

184 We can then apply this model repeatedly with leaders of increasing length  $L(t)$ ,  
 185 in order to approximate  $\lambda(s, t)$  for a growing leader channel. The time step at each point  
 186 in time will be  $\Delta t_k = \Delta s/v_k$ , where  $v_k$  is the speed of the leader growth at time  $t_k$ .

187 From the discrete charge distribution over time we can calculate the discretized cur-  
 188 rent by solving the continuity equation for  $I_i$  as

$$I_i(t_k) = -\Delta s \sum_{j=0}^i \frac{\lambda_j(t_k) - \lambda_j(t_{k-1})}{t_k - t_{k-1}} \quad (6)$$

189 Calculation of the electric field at the leader tip is somewhat nuanced because of  
 190 uncertainty about the effective channel radius  $r_C$ , so we will discuss this separately in  
 191 Section 3.2.

192 The leader tip potential drop  $\Delta\Phi_{tip}$  can also be calculated, it is simply defined as

$$\Delta\Phi_{tip} = \Phi_{cha} - \Phi_{amb}(s_{tip}) \quad (7)$$

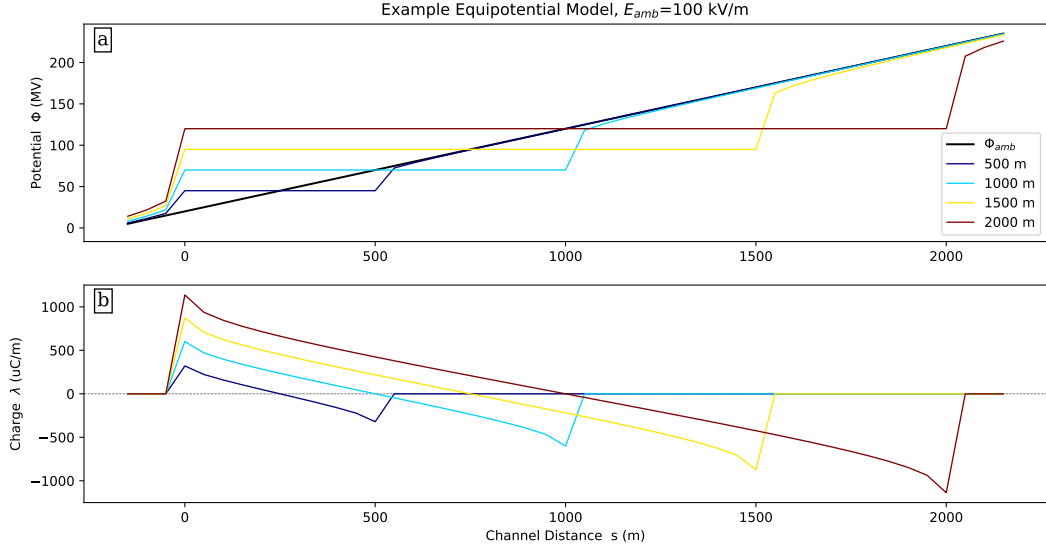


**Figure 1.** Examples calculations of the leader potential and charge distribution for various leader lengths in a uniform ambient field  $E_{amb} = 100$  kV/m, following the atmospheric electricity sign convention  $E = \nabla\Phi$ . Plots show the potential along the leader channel (a), and the induced charge distribution (b).

193 This is the difference between the channel potential and the ambient potential that would  
 194 exist at the tip if there was no leader present. Our  $\Delta\Phi_{tip}$  is similar to the definition of  
 195  $\Delta U_g^*$  in Celestin and Pasko (2011), or  $\Delta U_t$  in Bazelyan and Raizer (2000) (Equation 4.3  
 196 and other uses throughout). The potential drop  $\Delta\Phi_{tip}$  is generally proportional to the  
 197 tip field  $E_{tip}$ , but has the advantage that it does not depend on the tip geometry. Nev-  
 198 ertheless we will include  $E_{tip}$  estimates despite the much larger uncertainty because many  
 199 other papers on leader and streamer propagation consider average electric fields over some  
 200 distance rather than potential difference at a single point.

201 **EXAMPLE:** As an example of the model calculations, Figure 1 shows the leader  
 202 potential and charge distribution for a negative leader with  $r_C = 1$  m growing in a uni-  
 203 form ambient field  $E_{amb} = 100$  kV/m, following the atmospheric electricity sign con-  
 204 vention  $E = \nabla\Phi$ . The channel segment length is  $\Delta s = 50$  m. In this example the posi-  
 205 tive tip of the leader stays stationary, and the model values are plotted when the nega-  
 206 tive tip has reached distances of 500 m, 1000 m, 1500 m, and 2000 m. In Figure 1a the  
 207 potential is uniform within the channel, but the value of  $\Phi_{cha}$  increases as the negative  
 208 leader tip extends through the uniform field. In a uniform field  $\Phi_{cha}$  is equal to the po-  
 209 tential at the middle of the channel. Beyond the ends of the leader the potential quickly  
 210 returns to the ambient potential, as marked in black.

211 Figure 1b shows how the charge distribution changes as the leader propagates. In  
 212 a uniform field the leader has equal amounts of positive and negative charge at the tips,  
 213 tapering off to zero at the middle of the leader channel. As the leader propagates the  
 214 symmetry of the charge distribution remains, but the magnitude of the charge at either  
 215 end increases. Since only one tip is propagating in our example the zero charge point also  
 216 moves. In a uniform field the zero charge point is always halfway along the leader. For  
 217 an equipotential channel the induced charge  $\lambda(s)$  at each point is proportional to the dif-  
 218 ference between the channel potential  $\Phi_{cha}$  and the ambient potential at that point  $\Phi_{amb}(s)$ ,  
 219  $\lambda(s) \propto \Phi_{cha} - \Phi_{amb}(s)$  as pointed out originally by Kasemir (1960). So the point on  
 220 the leader with zero charge is the point where  $\Phi_{cha} - \Phi_{amb}(s) = 0$ , at the middle of

221 the channel in this case. There is a slight enhancement to the charge density  $\lambda(s)$  at the  
 222 tips of the leader, beyond the value expected by a  $\lambda(s) \propto \Phi_{cha} - \Phi_{amb}(s)$  relation. This  
 223 charge enhancement at the tips is related to the change in capacitance per unit length  
 224 at the tips of a cylinder (Jackson, 2000).

### 225 3.2 Leader Tip Electric Field

226 Having estimated the ambient field and associated charge density along the chan-  
 227 nel we also wish to estimate the electric field at the leader tip. Each segment of the leader  
 228 is a uniformly charged cylinder of length  $\Delta s$ , radius  $r_C$ , and linear charge density  $\lambda_i$ . From  
 229 first-principles electrostatics it can be shown that the electric field along the s-axis from  
 230 each cylindrical segment is given by

$$E_i(s) = \frac{\lambda_i}{2\pi r_C^2 \varepsilon_0} \left[ \sqrt{r_C^2 + s^2} + \Delta s - \sqrt{r_C^2 + (\Delta s + s)^2} \right] \quad (8)$$

231 where in this case  $s = 0$  is defined as the forward end of the cylinder, and the equa-  
 232 tion is only valid ahead of the cylinder in the direction of propagation ( $s \geq 0$ ).

233 Equation 8 demonstrates that the field for each segment drops off very quickly over  
 234 distances on the order of  $r_C$ . Thus, the field at the tip of the leader can be approximated  
 235 as due to just the final segment. This field is highest right at the edge of the cylinder,  
 236 so for  $s = 0$

$$E_{tip}(0) = \frac{\lambda_{tip}}{2\pi r_C^2 \varepsilon_0} \left[ r_C + \Delta s - \sqrt{r_C^2 + (\Delta s)^2} \right] \quad (9)$$

237 If we approximate Equation 9 using  $r_C^2 + (\Delta s)^2 \approx (\Delta s)^2$ , we get

$$E_{tip}(0) \approx \frac{\lambda_{tip}}{2\pi \varepsilon_0} \frac{1}{r_C} \quad (10)$$

238 Without further knowledge the effective capacitive radius  $r_C$  for a dart leader channel  
 239 could plausibly be anywhere from 1 mm to 100 m at the tip, so this  $1/r_C$  dependence  
 240 appears to pose a significant challenge in extracting any useful information about the  
 241 magnitude of the tip field.

242 However, the electric field at a single point in a highly non-uniform field is not re-  
 243 ally useful in any case. More relevant to a discussion about streamer or breakdown ac-  
 244 tivity at the tip would be the average field at the tip over some distance  $d$

$$\overline{E_{tip}}(d) = \frac{1}{d} \int_0^d \frac{\lambda_{tip}}{2\pi r_C^2 \varepsilon_0} \left[ \sqrt{r_C^2 + s^2} + \Delta s - \sqrt{r_C^2 + (\Delta s + s)^2} \right] ds \quad (11)$$

245

which evaluates to

$$\begin{aligned}
 \overline{E}_{tip}(d) &= \frac{\lambda_{tip}}{4\pi\epsilon_0 d} \left[ \ln \left( \frac{\sqrt{r_C^2 + d^2} + d}{r_C} \right) \right. & (A) \\
 &+ \ln \left( \sqrt{r_C^2 + \Delta s^2} + \Delta s \right) & (B) \\
 &- \ln \left( \sqrt{r_C^2 + (\Delta s + d)^2} + \Delta s + d \right) & (C) \\
 &- \frac{\Delta s + d}{r_C^2} \sqrt{r_C^2 + (\Delta s + d)^2} & (D) \\
 &+ \frac{d}{r_C^2} \sqrt{r_C^2 + d^2} & (E) \\
 &+ \frac{\Delta s}{r_C^2} \sqrt{r_C^2 + \Delta s^2} & (F) \\
 &\left. + \frac{2d\Delta s}{r_C^2} \right] & (G)
 \end{aligned} \tag{12}$$

246

where we have labeled each term (A, B, C, etc.).

247

248

249

Assuming  $\Delta s \gg d > r_C$  then (B) + (C)  $\approx 0$ . Applying the binomial approximation for  $\frac{r_C^2}{(\Delta s + d)^2} < 1$ ,  $\frac{r_C^2}{d^2} < 1$ , and  $\frac{r_C^2}{(\Delta s)^2} < 1$  to terms (D), (E), and (F) respectively, yields (D) + (E) + (F) + (G)  $\approx \frac{1}{4}$ . So we are left with

$$\overline{E}_{tip}(d) \approx \frac{\lambda_{tip}}{4\pi\epsilon_0 d} \left[ \ln \left( \frac{\sqrt{r_C^2 + d^2} + d}{r_C} \right) + \frac{1}{4} \right] \tag{13}$$

250

251

252

253

254

If we choose  $d = 1$  m then the difference in tip fields between  $r_C = 0.001$  m and  $r_C = 1$  m is about a factor of 7. This is still rather large, but at least gives an estimate of the tip field within about an order of magnitude, even across 3 orders of magnitude in radius. We do not use this approximation in the actual model calculations of  $E_{tip}$ , but it is useful for demonstrating the logarithmic dependency on  $r_C$ .

255

256

257

258

259

260

261

262

263

Additionally, the channel radius  $r_C$  is the effective radius of charge transported by streamers out into the corona sheath. The radius  $r_C$  should then approximately correspond to the radius at which the radial electric field is equal to the streamer stability field. Assuming the axial and radial fields are approximately equal, one should expect  $\overline{E}_{tip}(r_C)$  to be close to the value of the stability field. If this condition is met then we can be more confident that we have chosen  $r_C$  correctly and our calculated  $E_{tip}$  values are essentially correct. A more sophisticated model would allow  $r_C$  to vary so that the radial field was always equal to the streamer stability field for each segment (e.g. Cooray et al. (2009)), but for now a simpler model with fixed  $r_C$  is used.

264

265

266

267

268

269

270

We note that  $E_{tip}$  as discussed in this section is essentially the ‘‘vacuum solution’’ field as defined by Celestin and Pasko (2011), we are not accounting for streamers forming ahead of the conductive leader tip. Streamers ahead of the tip would reduce the field at the tip by spreading the potential drop  $\Delta\Phi_{tip}$  over a larger distance. Under typical approximations this would result in a constant  $E_{tip}$  equal to the streamer stability field  $E_{st}$ , which extends for a distance  $L = \Delta\Phi_{tip}/(2E_{st})$  (Bazelyan and Raizer (2000), page 69).

271

272

For  $E_{tip}$  in this paper we will report the values calculated from Equation 12 over a distance of  $d=1$  m.

273

### 3.3 Ambient Electric Field Estimation

274

275

276

277

278

For any ambient electric field distribution we can calculate the charge distribution along the channel with Equation 5. If we can map the channel path parameter  $s_i$  to 3D coordinates  $(x_i, y_i, z_i)$  in the sky we can then calculate the vertical electrostatic field at a point  $(X, Y, Z_{grnd})$  on the ground (where  $Z_{grnd}$  is the altitude of the ground above sea level) due to the charge distribution  $\lambda_i$  as:

$$E_z(X, Y, Z_{grnd}) = \sum_{i=1}^N \lambda_i \Delta s \frac{z_i - Z_{grnd}}{2\pi\epsilon_0 [(x_i - X)^2 + (y_i - Y)^2 + (z_i - Z)^2]^{3/2}} \quad (14)$$

279

280

281

282

283

where the ground is treated as an ideal infinite conducting plane. Since the lightning channel is far from our field measurement locations each segment of the channel can be approximated as a point charge. This calculation can be done for each time step  $t_k$  corresponding to a leader extension by  $\Delta s$ , to give the vertical field on the ground as a function of time,  $E_z(X, Y, Z_{grnd}, t_k)$ .

284

285

286

287

288

289

290

291

292

Typically for a lightning flash the ambient electric field  $E_{amb}(s)$  is not known, but the vertical electric field at the ground  $E_z(t)$  can be measured with an electric field change antenna. The extent of the conducting channel at any point in time can also be inferred from 3D lightning interferometer data. An initial guess can then be made for the ambient field  $E_{amb}(s)$ . For a conductive channel with endpoints at  $s_a(t_k)$  and  $s_b(t_k)$ , the charge distribution  $\lambda_i(t_k)$  induced by the guess  $E_{amb}(s)$  can be calculated from Equation 5. The corresponding field change at the ground  $E_z(t_k)$  can be calculated from Equation 14. The goodness-of-fit between the measured and modeled field changes can then be evaluated as

$$\chi^2 = \sum_{t_k} \frac{(E_{mod}(t_k) - E_{obs}(t_k))^2}{\sigma_k^2} \quad (15)$$

293

294

where  $E_{mod}(t_k)$  and  $E_{obs}(t_k)$  are the modeled and observed fields, respectively, at time  $t_k$ , and  $\sigma_k$  is the estimated uncertainty in the observed field.

295

296

297

298

299

300

301

302

303

304

We can then find the ambient electric field  $E_{amb}(s)$  which minimizes the  $\chi^2$  value iteratively using a non-linear optimization technique such as the Levenberg-Marquardt algorithm. The field on the ground does not depend strongly on each individual point  $E_{amb}(s_i)$ , so in order to limit the number of degrees of freedom we assume  $E_{amb}(s)$  takes the form of a polynomial of order  $n$ , rather than individually fitting each value of  $E_{amb}(s_i)$ . We also include a penalty in the  $\chi^2$  value for solutions where  $E_{tip}$  changes signs, since a real leader should stop propagating if this condition ever occurred. This penalty is chosen to be large enough to suppress sign changes in  $E_{tip}$ , but small enough that it does not upset the convergence of the solution or lead to significantly increased errors in Equation 15.

305

### 3.4 Model Implementation

306

307

308

309

310

311

Dart leader K-5 from Jensen et al. (2023b) was chosen to implement the model since this is a relatively simple IC dart leader. Figure 2 shows the known information for K-5, including the full 3D extent of the leader channel over time relative to the two fast antennas (FA01 and FA02), along with the electric field change vs time at the ground at these locations. This is the known information from which we want to estimate the unknown ambient electric field along the channel.

312

313

314

The leader path is simplified by smoothing the measured VHF source locations with a rolling average of the location over  $\pm 20 \mu s$ . Equally spaced and consecutive points  $\Delta s = 50$  m apart are selected to serve as the discrete leader segments in the model. The model

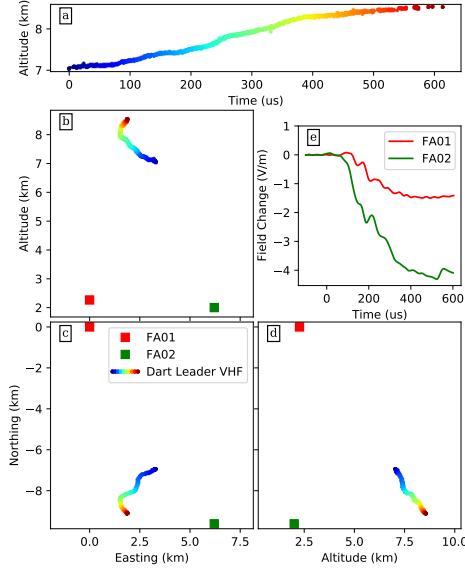


**Figure 2.** A plot of the path of the IC dart leader labeled K-5 over time relative to the two fast antennas. Panels are: altitude vs time (a), altitude vs easting (b), northing vs easting (c), and northing vs altitude (d). The points of K-5 are colored by time. The measured field change vs time at each station is also included (e), and the locations of the two fast antennas are marked in panels b, c, and d. The location of K-5 relative to the surrounding flash structure can be seen in Figure 3 of Jensen et al. (2023b).

315 includes a fixed channel radius of  $r_C = 1$  m to account for charge being transported  
 316 radially outward from the thin ( $\sim 1$  mm, (Rakov, 1998)) conducting core into the corona  
 317 sheath. To first order the capacitance of a long thin cylinder of length  $L$  and radius  $r_C$   
 318 is given by (Jackson, 2000):

$$C = \frac{2\pi\epsilon_0 L}{\ln(L/r_C)} \quad (16)$$

319 The dependence of the estimated background field on the channel radius is thus weak,  
 320 changing the modeled radius from 1 mm to 1 m only increases the capacitance by a factor  
 321 of 2 for a  $L=1$  km channel.

322 The channel of K-5 is obviously not perfectly straight. Since the axial field produced  
 323 by each cylindrical segment (Equation 8) drops off quickly over distances on the order  
 324 of  $r_C \ll \Delta s$ , only the nearest segments should contribute significantly to the potential  
 325 at each point along the leader channel. Thus we assume that Equation 1 is still valid  
 326 for the potential along a real tortuous leader channel as long the channel is approximately  
 327 straight over distances of a few times  $\Delta s$ . Since the channel is  $\sim 5$  km above the ground  
 328 we can ignore the contribution of image charges to the axial field along the channel.

329 We also assume that the dart leader channel starts with a conductive length of 100 m  
 330 at  $t=0$  in order to have some initial tip field and field change. Rather than skipping the  
 331 first 100 m of dart leader development, we use the 3D map of the full flash to find a path  
 332 along the same branch for 100 m in the direction opposite to the dart leader tip propa-  
 333 gation. Negative values of channel distance  $s$  correspond to this “backward” direction  
 334 along the branch. The negative dart leader tip starts at  $s = 0$  at time  $t = 0$ .

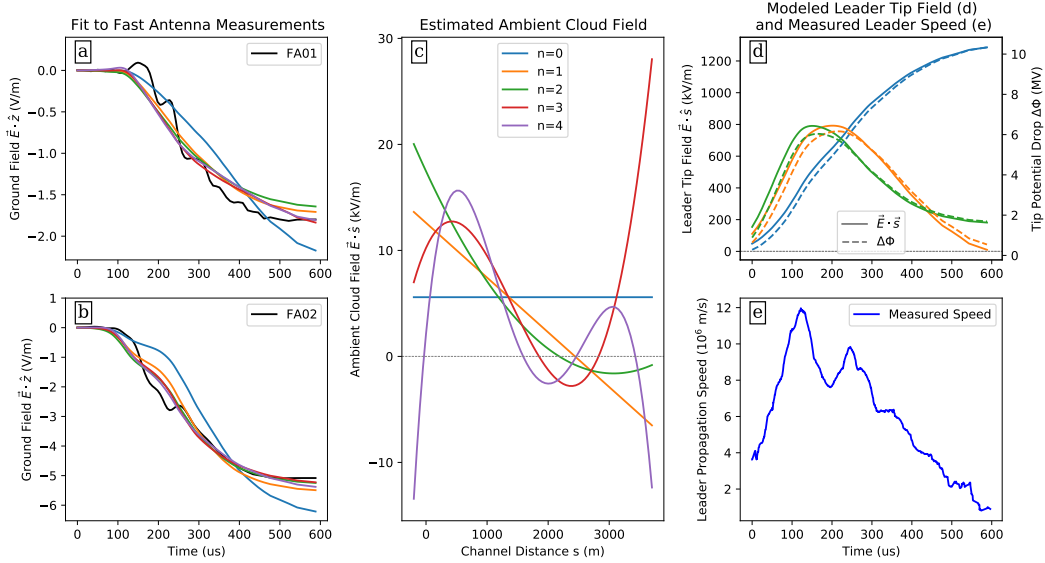


**Figure 3.** A plot of the modeled field change compared to the measured ground electric field change vs time (a and b), the estimated ambient cloud electric field vs channel distance (c), the estimated leader tip electric field  $E_{tip}$  vs time (d, left axis), and tip potential drop  $\Delta\Phi_{tip}$  vs time (d, right axis), for various degrees  $n$  of polynomial ambient fields. We plot  $|\Delta\Phi_{tip}|$  so the curves are not inverted compared to  $E_{tip}$ . The measured leader speed vs time (e) is included for comparison.

## 4 Results

### 4.1 Estimated Cloud and Tip Fields

All electric fields in plots use the atmospheric electricity sign convention, i.e. for the ambient cloud E-field and tip E-field a positive E-field will accelerate electrons in the direction of leader propagation,  $\hat{s}$ . Since the behavior of the negatively charged dart leader tip is the subject of interest this sign convention makes the plots easier to interpret.

Figure 3 shows the modeled field change (a and b) and estimated ambient field (c), where the ambient field is estimated using polynomials of various degrees  $n$ . The constant field ( $n = 0$ ) is clearly a worse fit to the measured field changes than the higher polynomial degrees that result in similar field changes. All the modeled field changes seem to only fit the slow components of the measured field change, up to about 5 kHz. This is true even if we drastically increase the allowed degrees of freedom (e.g.  $n = 50$ ). This suggests that the higher frequency components of the field change (above  $\sim 5$  kHz) are not associated with the general extension of the leader, but some other process which is not captured by our model. Since the higher frequency components do not seem to match between the two stations they may also simply be local interference at each station.

The polynomial ambient fields themselves (Figure 3c) generally decrease in the direction of dart leader extension as predicted in Jensen et al. (2023b) based on dart leader speed trends, although the initial and final field values in Figure 3c diverge quickly for  $n = 4$ , with the final field values also diverging for  $n = 3$ . The field behaviors in the  $n = 1$  and  $n = 2$  cases are similar and are more physically reasonable. We will specifically consider the  $n=2$  case for the rest of our analysis.

358 The ambient field values, which are mostly below 10 kV/m, are low compared to  
 359 typical thunderstorm fields which are often measured to reach 50-100 kV/m (Marshall  
 360 et al., 2001; Stolzenburg et al., 2007, 2015; Stolzenburg & Marshall, 2008). This is ex-  
 361 pected since the preceding leader, return stroke, and other discharge activities would have  
 362 zeroed-out the field along the channel, and the ambient field estimated here therefore  
 363 represents the recovery of the field along the channel as charge deposited in the corona  
 364 sheath continues to expand radially outward between strokes.

365 The sign-change of the field in Figure 3c ( $E_{amb} < 0$ ) is somewhat surprising, but  
 366 the charge re-distribution during a lightning flash is complex, and it is possible dart lead-  
 367 ers from other branches transported excess negative charge onto this branch while this  
 368 branch was otherwise decayed and non-conducting.

369 Figure 3d shows the modeled leader tip field  $E_{tip}$  (solid, left axis) and tip poten-  
 370 tial drop  $\Delta\Phi_{tip}$  (dashed, right axis) vs time. The  $n = 3$  and  $n = 4$  cases were omit-  
 371 ted to make the plot less cluttered. The curves for  $E_{tip}$  and  $\Delta\Phi_{tip}$  for a particular  $n$  value  
 372 are nearly identical up to a scaling factor. In Figure 3d  $|\Delta\Phi_{tip}|$  is plotted instead of  $\Delta\Phi_{tip}$   
 373 for comparison with  $E_{tip}$  and easier interpretation. The  $n = 1$  and  $n = 2$  cases have  
 374 an initial increase and gradual decreases of the tip field and potential drop, which is well  
 375 correlated with the measured speed vs time of K-5 (Figure 3e), supporting our claim in  
 376 Jensen et al. (2023b) that the leader speed is generally proportional to the leader tip field.  
 377 With the current polynomial field approach, the model is incapable of catching small de-  
 378 tails such as the speed dip at 200  $\mu s$ .

379 We include the  $n = 0$  case in Figure 3d to demonstrate that in a uniform field the  
 380 leader tip field and potential drop will increase indefinitely. The slope of the  $n = 0$   $E_{tip}$   
 381 vs time curve changes because leader length is converted to time using the observed leader  
 382 speed. The equipotential model itself is time independent, and  $E_{tip}$  is directly propor-  
 383 tional to leader length for a uniform field.

384 The tip field estimates are also lower than the traditional virgin air breakdown field.  
 385 At the height of 7-8 km, the breakdown field is expected to be  $E_k \cdot \delta \approx 1500$  kV/m,  
 386 where  $E_k = 3000$  kV/m for sea level air, and  $\delta$  is the air number density compared to  
 387 the sea-level/room temperature number density  $\delta = n(h, T)/n(h = 0km, T = 300K)$   
 388 (da Silva et al., 2019). However, for a preconditioned pre-dart-leader channel the tem-  
 389 perature may be significantly higher than 300 K, and the density will be correspondingly  
 390 lower. Following

$$\delta(h, T) \approx \frac{300}{T} e^{-h/10.4} \quad (17)$$

391 we have  $E_k \cdot \delta \approx 150$  kV/m for  $h=7$  km and  $T=3000$  K (Uman & Voshall, 1968), which  
 392 is closer to the leader tip fields we estimate at the start of propagation (Figure 3d). The  
 393 fact that the tip field never reaches the breakdown field for ambient air at 7 km may ex-  
 394 plain why dart leaders typically do not form new branches and instead follow the exist-  
 395 ing flash structure. The range of tip field values we found are generally in agreement with  
 396 the range of tip fields measured by Miki et al. (2002) in triggered lightning strikes, al-  
 397 though their measurements were made near sea level. The tip potential drop estimates  
 398 in Figure 3d are also in reasonable agreement with the “typical value” of 15 MV given  
 399 for dart leaders in Rakov and Uman (2003) Table 1.1.

400 The fact that the estimated leader tip field is initially lower than even the nom-  
 401 inal streamer stability fields in virgin air (500-750 kV/m at 7 km, (Babaeva & Naidis,  
 402 1997; Briels et al., 2008; Qin & Pasko, 2014)) may also explain the observation that the  
 403 width of dart leader channels resolved in VHF is much narrower than those of stepped  
 404 leaders (Hare et al., 2023a; Jensen et al., 2021; Shao et al., 2023). The fact that nega-  
 405 tive leaders are detected much more readily than positive leaders in VHF suggests that  
 406 the observed VHF predominantly comes from negative streamers. The axial field at the  
 407 leader tip ( $E_{tip}$ ) should also be the highest electric field at any point on the leader. So

408 if  $E_{tip}$  is below the negative streamer stability threshold in virgin air there should be no  
 409 negative streamers anywhere on the leader, except within the “warm” ( $\sim 1000$  K) pre-  
 410 conditioned channel core with a radius on the order of centimeters (Uman & Voshall,  
 411 1968), where the air density is lower. Recalling that  $E_{tip}$  is the average field over 1 m,  
 412 if  $E_{tip}$  is approximately equal to the virgin air stability field, and if the radial electric  
 413 field near the tip is approximately equal to  $E_{tip}$ , then we may expect streamers out to  
 414 a radius of about 1 m. This is in contrast to negative stepped leaders where  $E_{tip}$  is ex-  
 415 pected to be close to the breakdown field, and the streamer zone may have a radius of  
 416 10-100 m (Edens et al., 2014; Petersen & Beasley, 2013; Sonnenfeld et al., 2023).

417 In fact our streamer zone estimates agree very well with the high speed video ob-  
 418 servations of Petersen and Beasley (2013). While they observed a radial streamer/corona  
 419 zone of 10-20 m on a descending negative stepped leader, a later dart leader in the same  
 420 channel had no visible radial streamer zone, although there is some faint uniform lumi-  
 421 nosity which may be corona. Instead of a wide radial streamer zone the dart leader ex-  
 422 hibited a long forward streamer zone confined to the pre-conditioned channel, extend-  
 423 ing  $\sim 20$ -40 m ahead of the leader tip. This long forward streamer zone is expected. If  
 424 the air density in the pre-conditioned channel is  $\sim 1/10$ th the ambient density, then the  
 425 forward streamer zone within the pre-conditioned channel should be about 10 times longer  
 426 than the radial streamer zone.

427 As discussed in Section 3.2 there is a large uncertainty in the modeled tip field val-  
 428 ues due to the uncertainty in the effective channel radius  $r_C$ . For instance, the field val-  
 429 ues may be up to 7 times higher if the channel radius is 1 mm rather than 1 m. This would  
 430 make  $E_{tip}$  much higher than the streamer stability field for  $r_C=1$  mm. Recall however  
 431 that  $r_C$  is the effective radius of the channel due to streamers transporting charge into  
 432 the corona sheath. Our conclusions about the streamer zone radius based on  $E_{tip}$  should  
 433 therefore be consistent with our initial assumption of  $r_C$ . Since we infer a streamer zone  
 434 on the order of 1 m based on an assumption of  $r_C=1$  m our results are self consistent.

## 435 4.2 Speed, Tip Field, and Tip Current

436 Figure 4 shows a direct comparison between the measured leader speed, the mod-  
 437 eled tip field, and square root of the modeled tip current vs time for the  $n = 2$  case.  
 438 In the Figure we have normalized each variable to a maximum value of 1 to remove any  
 439 constants of proportionality. It is clear that the speed and tip fields are closely corre-  
 440 lated, except for the speed dip at 200  $\mu$ s and a small variation at the end. We do note  
 441 that the correlation is not as strong for other orders  $n$  of the polynomial ambient field,  
 442 and the correlation is also somewhat sensitive to how the errors are weighted in Equa-  
 443 tion 15 and model parameters. In fact, due to the ill-posed nature of the inverse prob-  
 444 lem there are essentially infinitely many ambient fields which could reproduce the mea-  
 445 sured field changes. Among these infinite solutions there are many possible ambient fields  
 446 which result in  $E_{tip}$  curves that do not match the leader speed, although many are phys-  
 447 ically unreasonable. While we cannot therefore definitively conclude that the leader speed  
 448 is proportional to the tip field as guessed in Jensen et al. (2021, 2023b), we can at least  
 449 claim that the observed field changes are consistent with a relationship of  $v \propto E_{tip}$  for  
 450 an equipotential leader.

451 If we frame the speed/field relationship as the leader mobility,  $v = \mu E$ , then we  
 452 get a value of  $\mu = 20$   $m^2/Vs$  for this particular dart leader. As shown in Figure 3d the  
 453 curves for  $E_{tip}$  and  $\Delta\Phi_{tip}$  are essentially identical up to a scaling factor, so the depen-  
 454 dence of the speed can be expressed in terms of either the tip field or potential drop. If  
 455 we model the tip speed as  $v = \eta\Delta\Phi_{tip}$  we get a value of about  $\eta = 2$  m/Vs.

456 Since there is a fair amount of uncertainty in the correlation between tip field and  
 457 speed we cannot completely rule out other power law relations such as the  $v = a\Delta\Phi_{tip}^{1/2}$   
 458 relation suggested by Bazelyan and Raizer (2000) Equation 4.2. We note that the value

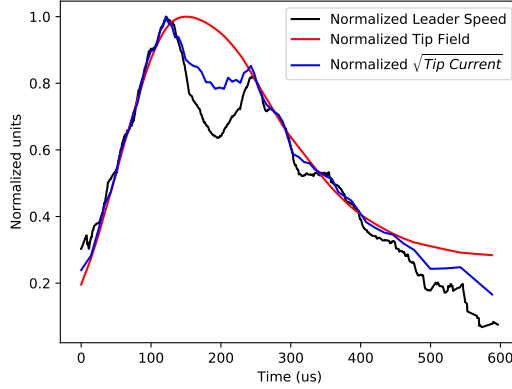


**Figure 4.** A plot of the normalized values of speed, tip field, and the square root of current vs time, for the  $n = 2$  fit.

459 of  $a = 15 \text{ m}/(\text{sV}^{1/2})$  suggested by Bazelyan and Raizer (2000) gives a speed 2 orders  
 460 of magnitude too low even if we assume the relationship can be adjusted as  $v = a\sqrt{\frac{\Phi_{tip}}{\delta}}$   
 461 for a 3000 K pre-dart-leader channel at 7 km altitude, where  $\delta$  is defined in Equation  
 462 17. Regardless of the form of the relation, our results do suggest that the tip electric field  
 463 or potential drop appears to be one of the main factors for the dart leader speed.

464 The square root of the tip current is also very well correlated with the speed in,  
 465 Figure 4, but this should not be surprising. If we re-write Equation 6 we can see that

$$I_{tip}(t_k) = -\Delta s \frac{\lambda_{tip}(t_k) - \lambda_{tip}(t_{k-1})}{t_k - t_{k-1}} = -\frac{\Delta s}{\Delta t} \lambda_{tip}(t_k) \quad (18)$$

466 where  $\Delta s/\Delta t$  is just the speed of the leader, and we are making use of the fact that  $\lambda_j(t_{k-1}) =$   
 467 0 for the advancing leader tip. This would suggest that  $I_{tip} \propto v$ , but we must further  
 468 consider that from Equation 12  $\lambda_{tip} \propto E_{tip}$ , so we must have  $I_{tip} \propto vE_{tip}$ . We have  
 469 also just established that  $v \propto E_{tip}$ , so therefore  $I_{tip} \propto v^2 \propto E^2$  is exactly the form we  
 470 should expect. This result also generally agrees with numerical modeling of the streamer  
 471 to leader transition by da Silva and Pasko (2013), and empirical relations based on labor-  
 472 atory sparks suggested by Andreev et al. (2008) and Bazelyan and Raizer (1997)(page  
 473 213). Rather than implying that higher current somehow causes a higher speed, it is likely  
 474 that the causal relationship is the other way around. A faster dart leader will generally  
 475 be changing in potential more quickly, both at the tip and along the entire leader length,  
 476 and this potential change will induce a larger current.

### 477 4.3 Other Model Results

478 Figure 5 shows the modeled potential, charge density, and current distributions along  
 479 the leader colored by time, for the  $n = 2$  model. Each curve in Figure 5 is a snapshot  
 480 of conditions along the entire plotted distance at a particular time indicated by the color.  
 481 Ahead of the negative leader tip at any point in time the charge and current are zero,  
 482 and the potential is just the ambient potential. Thus in each plot a sharp increase along  
 483 a curve of a particular color at a positive channel distance indicates the position of the  
 484 negative leader tip at that time. Some distance past the positive tip of the leader (in the  
 485  $-s$  direction) is also included to show the return to ambient conditions on that end.

486 Figure 5a shows that the potential along the active part of the channel is always  
 487 a horizontal line due to the equipotential assumption, and the overall channel potential  
 488 is increasing over time as the leader grows in length. If we consider the dart leader as

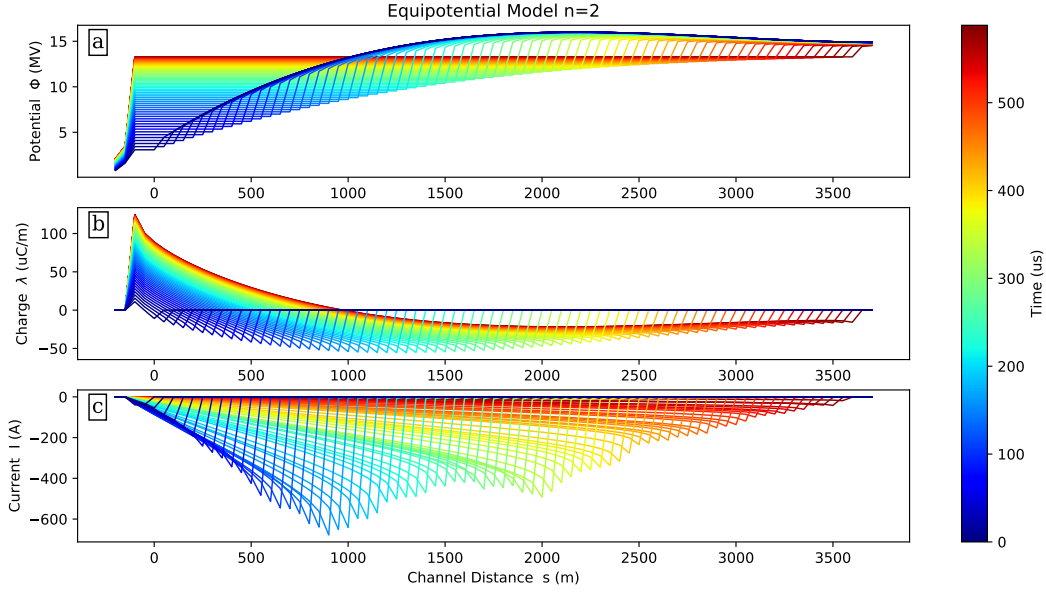


**Figure 5.** Plot of the potential distribution (a), charge density distribution (b), and current distribution (c) along the leader channel, colored by time, for the  $n = 2$  polynomial ambient field. In all three plots the sharp increase at the leading edge indicates the leader tip position at that time.

489 transporting negative charge while leaving relatively stationary positive charge behind  
 490 then this increase in channel potential over time corresponds to an overall decrease in  
 491 potential energy, as expected. Ahead of the leader tip the potential essentially returns  
 492 to the ambient potential within one step  $\Delta s$ . We can also see that the charge distribu-  
 493 tion (Figure 5) essentially satisfies  $\lambda(s) \propto \Phi_{cha} - \Phi_{amb}(s)$ .

494 The amount of charge at the negative leader tip in Figure 5b does increase initially  
 495 as in our simple dipole model in Jensen et al. (2023b), but then the charge at the tip de-  
 496 creases somewhat as the leader progresses. However, there is a larger deposit of charge  
 497 behind the tip which remains more constant, this may be the cause of the nearly con-  
 498 stant tip charge in our previous dipole model as the leader slowed to a stop (Jensen et  
 499 al., 2023b). The charge density at the positive tip on the other hand increases contin-  
 500 ually as the leader progresses, although the increase is fastest at the beginning. The scale  
 501 of the charge density at tens of  $\mu\text{C}/\text{m}$  is much smaller than typical charge density es-  
 502 timates of about  $1 \text{ mC}/\text{m}$ , but these estimates are typically for stepped leaders in vir-  
 503 gin air, where the ambient fields (and thus charge density) are much higher.

504 The current in Figure 5c is highest right at the negative tip. For a more realistic  
 505 channel with some finite conductivity we would expect this peak to follow a little behind  
 506 the leader tip as the charge density at the tip takes some finite time to build. The cur-  
 507 rent then drops off towards the stationary positive tip of the leader since the potential  
 508 is not changing as much at that end. The peak current magnitude is about 700 A, which  
 509 is in reasonable agreement with the “typical” dart leader current of 1 kA given in Rakov  
 510 and Uman (2003) Table 1.1.

## 5 Discussion

### 5.1 Validity of the Equipotential Assumption

Our modelling results assume a perfect equipotential channel, therefore the conclusions we draw about dart leader propagation are only valid if real dart leader channels are approximately equipotential. In this section we put forward three arguments that dart leader channels are approximately equipotential, and that our modeling results are therefore valid.

First, a channel with finite conductivity  $\sigma_R$  will approach an equipotential over time, so the key question is how the time scale at which the channel reaches equipotential compares to the timescale of the leader propagation.

For a channel of length  $L$  and conductive/resistive radius  $r_R$  the total channel resistance is given by

$$R = \frac{L}{\sigma_R \pi r_R^2} \quad (19)$$

We can then estimate the timescale at which the leader approaches equipotential as  $\tau \approx RC/10$  (see Appendix A for a derivation). Writing the equation out fully combining Equations 16 and 19 we have

$$\tau \approx \frac{1}{10} \frac{2\pi\epsilon_0 L}{\ln(L/r_C)} \frac{L}{\sigma_R \pi r_R^2} \quad (20)$$

This time constant is derived assuming a channel of fixed length  $L$  suddenly becomes conductive in a uniform field, which does not really match the conditions of an extending channel in a non-uniform field, but it is still useful to consider the results of this simple approximation.

High speed spectroscopy observations of dart leaders suggest that they reach temperatures of  $\sim 20$  kK (Chang et al., 2017; Orville, 1975), which corresponds to equilibrium conductivity  $\sigma_R$  of about  $10$  kS/m (Chang et al., 2017; Yos, 1963). The conductive radius  $r_R$  of a dart leader channel is estimated to be about 1-4 mm (Rakov, 1998), and for a well developed dart leader it is likely to be closer to 4 mm. The channel for K-5 is about 3500 m long by the end of its propagation, so with  $r_R=4$  mm and  $\sigma_R=10 \times 10^3$  ( $\Omega m$ )<sup>-1</sup> we get a time constant of  $\tau=10$   $\mu s$ . Since 10  $\mu s$  is short compared to the propagation timescale of dart leaders (100-1000  $\mu s$ ) the dart leader channel should be close to equipotential, at least by the time it stops propagating.

As a second argument,  $\tau$  is also an estimate of how long it should take the field change to stop after propagation ceases. Any significant current in the channel will lead to a changing field at the ground. Ohm's Law  $j = \sigma E$  suggests that the current will only drop if either the field or conductivity drops by several orders of magnitude. The channel conductivity is kept high by current heating the channel, so we should not expect the conductivity to drop while there is still significant current on the channel. Thus for a hot plasma channel the current will only stop when the field along the channel drops to essentially zero. Therefore the channel must be close to an equipotential when the field on the ground has stopped changing, and  $\tau$  must also be low enough to allow the channel to reach equipotential by this time. Since the measured fields in Figures 3a and b have essentially stopped changing even before the leader has stopped propagating, we can assume that the leader is in fact close to an equipotential.

Finally, we consider the non-linear resistance of a plasma channel. For a plasma channel to remain hot and conductive ohmic heating must balance heat losses. The associated resistance will cause the current in the channel to be somewhat less than the ideal equipotential current, and the channel will take longer to reach the equipotential charge distribution. Therefore there will be some remaining potential gradient along the

556 channel  $\nabla\Phi_{cha}$ . We emphasize that in lightning  $\nabla\Phi_{cha}$  is ultimately caused by the am-  
 557 bient potential gradient  $\nabla\Phi_{amb}$ .

558 Laboratory experiments of free burning arcs suggest that for currents of about 100 A  
 559 to 1000 A the steady state potential gradient is between 1 kV/m (King, 1962; Mazur &  
 560 Ruhnke, 2014) and 2.5 kV/m (Montano et al., 2006). These potential gradients are small  
 561 enough that they should not significantly change our results. To verify this we model dart  
 562 leader K-5 while including such a potential gradient. We set the channel potential gra-  
 563 dient  $\nabla\Phi_{cha}$  to be equal to the constant gradient  $\nabla\Phi_{const}$  as long as the resulting  $\Phi_{cha}(s)$   
 564 is between  $\Phi_{amb}(s)$  and the ideal equipotential value at each point. Otherwise the chan-  
 565 nel remains at  $\Phi_{cha}(s) = \Phi_{amb}(s)$ . In keeping with our second argument for the equipot-  
 566 ential model, we allow  $\nabla\Phi_{cha}$  to approach zero as the leader slows to a stop. Based on  
 567 Figure 11 of Montano et al. (2006) we drop  $\nabla\Phi_{cha}$  to zero linearly over about 350  $\mu$ s.  
 568 Figures in the format of Figures 3 and 5 are included in the supporting information for  
 569  $\nabla\Phi_{const}=2.5$  kV/m. We show the  $n = 1$  ambient field because the  $n = 2$  case has con-  
 570 vergence issues when including the potential gradient. The results shown in those plots  
 571 are very similar to the ideal equipotential results. Therefore the results of our equipot-  
 572 ential modeling are a good approximation of the true leader properties even if a real leader  
 573 has some internal potential gradient.

## 574 5.2 Branch Junctions

575 In Jensen et al. (2023b) we hypothesized that the rapid speed variations as dart  
 576 leaders passed branch junctions may be caused by charge deposits near those junctions.  
 577 The negative dart leader tip would be repelled by a negative charge deposit near the junc-  
 578 tion, so that the dart leader might decelerate while approaching the junction and accel-  
 579 erate after passing it. It is clear from the results in Section 4 that rapid variations in the  
 580 ambient field are not resolved based purely on fitting to the measured field changes at  
 581 the ground.

582 In order to test our branch junction hypothesis explicitly we need to modify our  
 583 approach. Since the results in Section 4.2 do suggest a correlation between the tip field  
 584  $E_{tip}$  and the leader speed, we add this as another constraint using our assumed relation-  
 585 ship of  $v = \mu E_{tip}$ , leading to a  $\chi^2$  value

$$\chi_{speed}^2 = \sum_{t_k} \frac{(\mu E_{tip}(t_k) - v_{obs}(t_k))^2}{\sigma_{speed}^2} \quad (21)$$

586 We also add a term to the ambient field which corresponds to the charge config-  
 587 uration in Figure 6. For a branch junction at location  $s_{junc}$  with a point charge  $q_{junc}$   
 588 at a distance  $h_{junc}$  along the perpendicular second branch the resulting electric field on  
 589 the leader channel is

$$E_{junc}(s) = \frac{q_{junc}}{4\pi\epsilon_0} \frac{s - s_{junc}}{[(s - s_{junc})^2 + h_{junc}^2]^{3/2}} \quad (22)$$

590 where we are treating the channel as perfectly straight for simplicity, and calculating the  
 591  $\vec{E}_{junc} \cdot \hat{s}$  component of the field.

592 To avoid having the junction charge significantly modify the field fit away from the  
 593 junction, we find the fitting parameters in two stages. First  $h_{junc}$  and  $q_{junc}$  are fit us-  
 594 ing the Levenberg-Marquardt algorithm, while using an assumed value of  $s_{junc}=1675$  m  
 595 since this is where the change in speed is observed along the channel. As a background  
 596 field the same  $n = 2$  ambient field previously found in section 4 is used. The value of  
 597  $\mu = 20$  m<sup>2</sup>/(Vs) from Section 4.2 is also used so that the proportionality between the  
 598 speed and tip field remains the same. The time range of Equation 21 is limited to  $t =$   
 599  $100$   $\mu$ s to  $t = 260$   $\mu$ s, since this is the range of the dip in observed speed. This way we

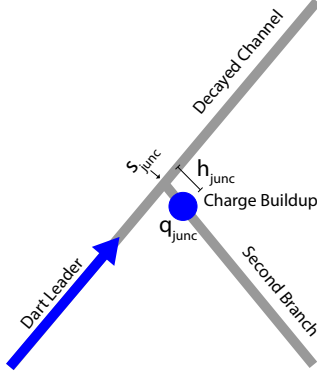


**Figure 6.** A diagram showing the configuration of the branch junction charge. The junction between branches is located at a point  $s_{junc}$ . A charge  $q_{junc}$  is located a perpendicular distance  $h_{junc}$  away from the junction point, along the second branch.

600 are fitting the dip specifically without trying to optimize the fit for other times. For the  
 601 fast antenna field change fit we continue to use the full time range. The combined good-  
 602 ness of fit parameter is then  $\chi_{tot}^2 = \chi_{FA01}^2 + \chi_{FA02}^2 + \alpha\chi_{speed}^2$  where  $\alpha$  is a weighting  
 603 term which we adjusted manually to achieve a reasonable balance between fitting the  
 604 field change and the speed.

605 After finding a reasonable fit for the junction point charge parameters, we then re-  
 606 fit the background field with a 2nd order polynomial in order to find a better fit with  
 607 both terms present. This process could be repeated iteratively, alternating between junc-  
 608 tion charge and background field fits, but we found one iteration was enough in this case.  
 609 It may also be possible to fit the junction charge and background field both at the same  
 610 time, but due to issue with convergence to the optimal result and the need for human  
 611 judgement in weighting the  $\chi^2$  values the two stage approach was more tractable.

612 The results from this process are shown in Figure 7. Figures 7a and 7b show only  
 613 a modest change in the modeled field change at the ground from the  $n = 2$  results in  
 614 Figures 3a and 3b. The ambient field in Figure 7 includes the 2nd order polynomial back-  
 615 ground field, the junction charge field from Equation 22, and the sum of the two field  
 616 terms. The fit values are  $h_{junc}=332$  m and  $q_{junc}=-115$  mC. The tip field and tip po-  
 617 tential drop vs time in Figure 7d show a pronounced dip around the location of the dip  
 618 in speed in Figure 7e. We further include the modeled  $v = \mu E$  in Figure 7e, this model  
 619 slightly over-estimates the speed but in general there is now an excellent agreement with  
 620 the measured leader speed for the whole leader duration.

621 We note that there is no branch visible in the BIMAP-3D sources at the  $s_{junc}=1675$  m  
 622 location of the simulated charge, even when we include all VHF sources from the full recorded  
 623 flash. There are multiple small side branches within a few hundred meters of this loca-  
 624 tion that appear in VHF either before or after K-5, and possibly the speed variation we  
 625 observe is due to the combined influence of these multiple side branches. It is also possi-  
 626 ble that some previous leader activity deposited charge directly along the channel with-  
 627 out the need for a branch junction. Either way, we have at least demonstrated that our  
 628 hypothesis from Jensen et al. (2023b) is generally viable. We have reinforced our con-  
 629 clusion from Section 4.2 that using the equipotential model a leader speed relationship  
 630 of  $v = \mu E_{tip}$  is consistent with both our observations of field changes at the ground and  
 631 the observed leader speed. Further, under the equipotential model it is possible for a charge  
 632 deposit a relatively short distance from the primary channel to cause  $E_{tip}$  to exhibit a

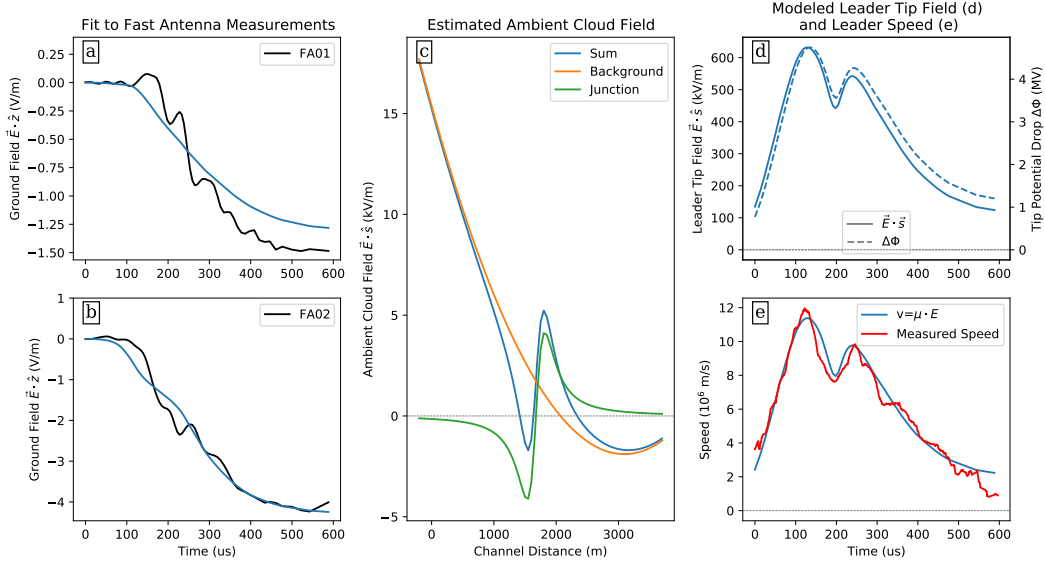


**Figure 7.** Equipotential model results when adding the junction charge term to the  $n=2$  ambient field from Section 4. In the same format as Figure 3, the plot shows the measured and fit field change vs time for FA01 (a) and FA02 (b), the ambient field vs channel distance (c) including the background 2nd order polynomial field, the junction charge field, and the sum of these two components. The leader tip field vs time (d, left axis) and tip potential drop vs time (d, right axis) is shown, along with the measured and modeled leader speed vs time (e).

633 rapid drop and recovery, like the branch junction speed changes reported in Jensen et  
 634 al. (2023b), without significantly changing the field change measured at the ground.

635 We note that the fit presented in Figure 7a seems to slightly under-estimate the  
 636 magnitude of the field change for FA01, but this could be due to the large uncertainty  
 637 in gain calibration for each fast antenna. A similar underestimation does also occur in  
 638 Figure 3a but it is less obvious since multiple modeled field changes are shown. Addi-  
 639 tionally, in Figure 7a different values of  $\mu$  might allow a better simultaneous fitting of  
 640 the speed and field changes. Since this is a first-of-its-kind comparison of the equipoten-  
 641 tial model with observed 3D leader propagation, and since the uncertainties in fast anten-  
 642 na calibration are so large, we will not attempt to refine the fit further.

### 643 5.3 Bidirectional Development

644 High speed camera observations of dart leaders initiating outside of clouds indi-  
 645 cate that the bright channel initially extends bidirectionally, but the extension in the pos-  
 646 itive tip direction quickly halts once it reaches the previously observed end of the pre-  
 647 conditioned channel (Ding et al., 2024; Mazur, 2016). Unfortunately this extension in  
 648 the positive direction is not observed in VHF by BIMAP-3D. We have performed some  
 649 tests assuming the positive tip extends at the same speed as the negative tip until it reaches  
 650 the end of the channel as observed in earlier VHF.

651 Plots showing the K-5 results when including this bidirectional development are  
 652 included in the supporting information, in the style of Figures 3 and 5. The estimated  
 653 ambient field is somewhat lower in magnitude when including bidirectional development,  
 654 but still generally decreases in the direction of propagation. The modeled leader tip field  
 655 is slightly lower, peaking at about 500 kV/m rather than 800 kV/m, but it is still gen-

erally correlated with the leader speed. Thus the inclusion of this bidirectional development does not significantly change any of our conclusions. The most significant change is that the current is high at both leader tips while they are propagating, with a more uniform current through the middle of the channel. After the positive tip stops propagating the current distribution is similar to the distribution shown in Figure 5.

Figure S3d in the supporting information also includes the tip field and potential drop for the positive tip of the dart leader. The positive tip field is below the ambient air breakdown field. This explains why the fast bidirectional development stops once it reaches the end of the pre-conditioned channel. As reported by Jensen et al. (2023b) the positive tip appears to continue extending at  $2 \times 10^4$  m/s throughout the dart leader phase of the flash. Our new modeling results suggest this  $2 \times 10^4$  m/s positive tip extension may occur with a tip field above the positive streamer stability threshold but below the breakdown field in virgin air.

In a few cases for other dart leaders shown in the supporting information (most notably K-2) significant bidirectional development needs to be added to the model in order to match the field change at both stations. This suggests that there was more bidirectional development for those dart leaders, as compared to some of the other dart leaders where adding a bidirectional component made little difference to the field change or speed fits. The differences seem to be both in the geometry of the channel and in the overall shape of the resulting field change.

#### 5.4 Other Dart Leaders

We also estimated ambient fields and tip fields for several other IC dart leaders from the same flash analyzed in Jensen et al. (2023b). Figures for these are included in the supporting information to avoid an excessive number of figures in the main text. We excluded a few cases where the dart leader development involved multiple simultaneous branches (K-10 and K-14), or there were large gaps in time with no located VHF sources (K-7) since our methodology depends on the leader following one single path with a well defined tip location at each point in time. For a few other dart leaders which split into multiple branches we were able to model the initial portions before they branched (K-4 and K-9). These are marked as “partial” fits. The path each dart leader follows can be seen in the figures of Jensen et al. (2023b), or the figures and animations in the supplementary material for that paper (Jensen et al., 2023a).

For the other dart leaders we explicitly look for an ambient field which fits both the measured field changes and the measured leader speed. We do this by adding the  $\chi_{speed}^2$  term from Equation 21, although in some cases this additional constraint seems to cause convergence issues for the Levenberg-Marquardt algorithm, and we actually obtained better fits to the leader speed without the explicit  $\chi_{speed}^2$  constraint. We allow the  $\mu$  value to be determined as the median value of  $v(t_k)/E_{tip}(t_k)$  for each iteration.

In most cases shown in the supporting information we were able to find ambient fields such that the modeled leader fit both the measured field changes, while also having a tip field which was generally correlated with the leader speed. In all these valid cases the estimated cloud field generally decreases along the channel length, similar to Figure 3c. The highest field values are also similarly low, less than about 10 kV/m, with the exception of K-3 which peaks at about 45 kV/m. If K-3 is modeled with equal development in the positive and negative directions then the estimated ambient field peaks at  $<20$  kV/m, while the field change remains similar, and the tip field is actually slightly better correlated with the leader speed. The modeled  $E_{tip}$  values are much lower for K-3 if we assume the leader extension is symmetrical about the starting point.

Among the valid cases the tip field and leader speed correlations ranged from being quite close to only being vaguely correlated. These generally support our conclusion

706 that the observed leader speed trends can be explained as  $v \propto E_{tip}$  for an equipoten-  
 707 tial leader, especially considering we are estimating the ambient field with only a few de-  
 708 grees of freedom, so we cannot expect to match complicated variations in speed. It may  
 709 be possible to allow more degrees of freedom while fitting to the leader speed in addi-  
 710 tion to the measured field changes, but in our testing there seemed to be issues converg-  
 711 ing to an optimal solution. A more robust approach might be to start with a simple lin-  
 712 ear ambient field fit and then use the linear field as an initial guess while gradually adding  
 713 degrees of freedom. Adding degrees of freedom as piece-wise linear fits rather than poly-  
 714 nomials might also improve the convergence behavior, while avoiding the undesirable poly-  
 715 nomial divergence near the endpoints.

716 For the empirical relation  $v = \mu E_{tip}$  we find  $\mu$  values ranging between 10-30 m<sup>2</sup>/Vs.  
 717 For the relation  $v = \eta \Delta \Phi_{tip}$  we find  $\eta$  values ranging between 1-4 m/Vs. For K-4 we  
 718 find extreme outlier values of  $\mu$  and  $\eta$ , but the net field change in K-4 is a small frac-  
 719 tion of the noise level, so the results are not reliable. Since our uncertainties are large  
 720 and the quality of fit varies for each leader we cannot say whether the differences in these  
 721 values among different dart leaders are caused by random uncertainty, or if they reflect  
 722 something more fundamental like the temperature of the pre-dart-leader channel in each  
 723 case.

724 In a few cases (the full K-8 and K-13) we were not able to match the measured field  
 725 changes from both stations. These cases indicate that it is possible for a dart leader to  
 726 have a more complicated field change even if the observed development in VHF seems  
 727 fairly simple. Comparing the field change timing (supporting information for this pa-  
 728 per) to the leader development (Jensen et al., 2023a), for both K-8 Full and K-13 the  
 729 shift towards a positive field change at FA02 occurs close to the time that those dart lead-  
 730 ers reach junction J1. This strongly indicates that the more complicated field changes  
 731 are caused by VHF invisible development into the other branch at J1. For these cases  
 732 where the measured field changes at the ground could not be reproduced the correspond-  
 733 ing model results are not valid. These cases are included only to show that while our equipo-  
 734 tential model constrained by the BIMAP-3D observations works in most cases, there are  
 735 some exceptions.

## 736 6 Summary

737 Due to the integral nature of the field change at the ground in Equation 14, there  
 738 are essentially an infinite number of ambient field solutions which will fit the observed  
 739 field changes, even when constrained by the path and speed of leader development as ob-  
 740 served by BIMAP-3D. Solving for this ambient field is thus an “ill-posed” inverse prob-  
 741 lem. The dart leader channel properties we model are therefore not definitive, but are  
 742 at least consistent with our observations. The fact that our modeled results seem to ex-  
 743 plain more general observed properties of dart leaders, and the fact that we obtained most  
 744 of these model results using only simple linear or quadratic ambient fields lends further  
 745 credibility to our claims.

746 The following conclusions are consistent with our observations:

### Section 4.1

- 748 1. A physically plausible ambient field  $E_{amb}$  which matches VHF observations of chan-  
 749 nel development and electric field changes at the ground can be found
- 750 2. The estimated ambient field along the dart leader channel is generally low, less  
 751 than 15 kV/m
- 752 3. The ambient field generally decreases in the direction of dart leader propagation
- 753 4. The modeled  $E_{tip}$  and  $\Delta \Phi_{tip}$  are essentially proportional to each other
- 754 5.  $E_{tip}$  is generally less than  $E_k \cdot \delta$  unless the pre-dart-leader channel has a signif-  
 755 icantly elevated temperature ( $\sim 1000-3000$  K) compared to ambient air

- 756 6. Dart leaders are typically confined to pre-conditioned channels because their tip  
 757 fields are too low to propagate into virgin air ( $E_{tip} < E_k \cdot \delta$ )  
 758 7. The modeled  $E_{tip}$  values are close to the negative streamer stability field in amb-  
 759 760 761 762

**Section 4.2**

- 764 8.  $E_{tip}$  and  $\Delta\Phi_{tip}$  are correlated with the observed leader propagation speed  
 765 9. The square root of the current at the leader tip is also correlated with leader speed,  
 766 this is expected since the model equations yield  $I_{tip} \propto v \cdot E_{tip}$  and we have ob-  
 767 768

**Section 4.3**

- 769 10. The equipotential model allows calculation of the potential of the leader channel,  
 770 as well as the charge and current distributions, all resolved in time and space

**Section 5.1**

- 772 11. The equipotential model is a good approximation of the true leader properties

**Section 5.2**

- 774 12. A charge deposit near the channel can produce tip field variations similar to the  
 775 speed variations we observed associated with branch junctions in Jensen et al. (2023b)

**Section 5.3**

- 777 13. In most cases including some initial bidirectional extension in the dart leader de-  
 778 779 780 781 782 783 784 785 786

**Section 5.4**

- 788 17. Similar results can be obtained for several other dart leaders from the same flash  
 789 18. For the empirical relation  $v = \mu E_{tip}$  we find typical values of  $\mu=10-30$  m<sup>2</sup>/Vs  
 790 19. For the empirical relation  $v = \eta \Delta\Phi_{tip}$  we find typical values of  $\eta=1-4$  m/Vs  
 791 20. In a few cases the model cannot fit the observed field changes at both stations si-  
 792 793

**Appendix A Time Constant Derivation**

795 To first order, the self-capacitance  $C_{tot}$  of a long cylindrical leader channel is given  
 796 by Equation 16. The total resistance  $R_{tot}$  of the channel is then given by Equation 19.  
 797 If we split this leader channel into  $N$  discrete segments then each segment has capaci-  
 798 799 800

801 If the leader is initially non-conductive in a uniform electric field, and then sud-  
 802 803 804 805

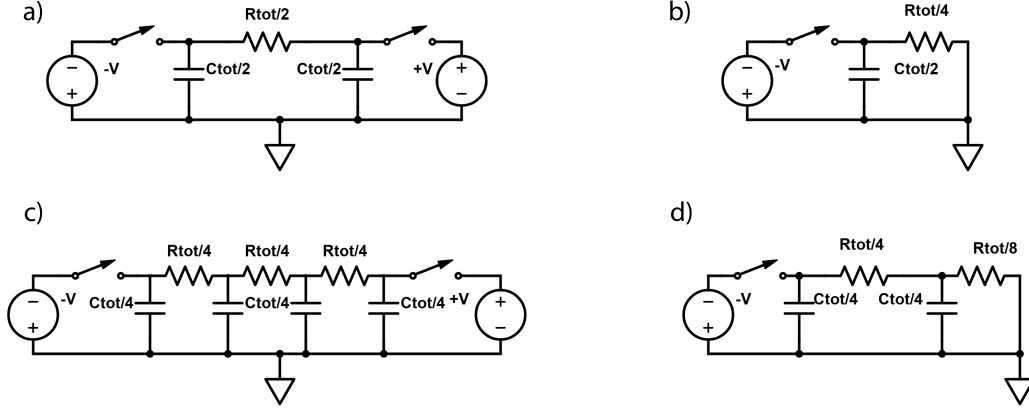


**Figure A1.** Circuit diagram showing the  $N=2$  (a, b) and  $N=4$  (c, d) simple model of a leader in a uniform field as  $N$  capacitors connected by  $N-1$  resistors, with the capacitors driven by equal and opposite voltages across switches. On the right (b, d) we see the equivalent circuits reduced by symmetry.

806 First we consider the simple case of  $N=2$  segments. We then have an electrical circuit  
 807 with two capacitors of value  $C = C_{tot}/2$ , separated by a resistor of value  $R = R_{tot}/2$ ,  
 808 as shown in Figure A1a. If this circuit is driven by equal and opposite voltages  $+V$  and  
 809  $-V$  (analogous to a leader channel in a uniform field), then by symmetry the voltage must  
 810 always be 0 in the middle of the resistor, and the circuit in Figure A1a is equivalent to  
 811 the circuit in Figure A1b (up to the sign of the voltage). The circuit in Figure A1b is  
 812 a regular RC circuit, so we can immediately see that the time constant is  $\tau = (R_{tot}/4)(C_{tot}/2) =$   
 813  $R_{tot}C_{tot}/8$ . For  $N=2$  our choice of  $R = R_{tot}/2$  is somewhat contrived, but as  $N$  gets  
 814 larger the difference between  $R_{tot}$  and  $R_{tot}(N-1)/N$  becomes negligibly small.

815 We then consider the  $N=4$  case, shown in Figure A1c. Again by symmetry we can  
 816 see that the voltage at the center of the middle resistor must always be zero, and thus  
 817 the discharging circuit is equivalent to Figure A1d. After applying Kirchoff's node law  
 818 for this circuit and substituting the relevant terms in voltage and  $\frac{dV}{dt}$  we get a system  
 819 of ordinary differential equations

$$\frac{dV_1}{dt} = \frac{16}{R_{tot}C_{tot}} (-V_1 + V_2) \quad (\text{A1})$$

$$\frac{dV_2}{dt} = \frac{16}{R_{tot}C_{tot}} (V_1 - 3V_2) \quad (\text{A2})$$

820 where  $V_1$  is the voltage of the capacitor closest to the voltage source and  $V_2$  is the ca-  
 821 pacitor closest to the ground point.

822 This system of differential equations can be re-framed as an eigenvalue problem by  
 823 writing the system as

$$\frac{d}{dt} \begin{bmatrix} V_1 \\ V_2 \end{bmatrix} = \frac{16}{R_{tot}C_{tot}} \begin{bmatrix} -1 & 1 \\ 1 & -3 \end{bmatrix} \begin{bmatrix} V_1 \\ V_2 \end{bmatrix} \quad (\text{A3})$$

824 which has a solution of the form

$$\vec{V} = \vec{X}e^{\lambda t} \quad (\text{A4})$$

825 where  $\vec{X}$  is an eigenvector and  $\lambda$  is the corresponding eigenvalue of the matrix in Equa-  
 826 tion A3. In this case the eigenvalues and corresponding eigenvectors are

$$\lambda = \frac{16}{R_{tot}C_{tot}} (\pm\sqrt{2} - 2); \quad \vec{X} = \begin{bmatrix} 1 \pm \sqrt{2} \\ 1 \end{bmatrix} \quad (\text{A5})$$

827 The full solution will be a linear combination of solutions of the form given in Equa-  
 828 tion A4 for the two eigenvalue/eigenvector pairs, but for our purposes we are interested  
 829 only in the time constants. The slower time constant will dominate over longer times,  
 830 this time constant is

$$\tau = \frac{R_{tot}C_{tot}}{16(2 - \sqrt{2})} \approx \frac{R_{tot}C_{tot}}{9.37} \quad (\text{A6})$$

831 Checking higher orders of N with numerical simulations we find that the decay time  
 832 remains within the range

$$\frac{R_{tot}C_{tot}}{8} < \tau < \frac{R_{tot}C_{tot}}{10} \quad (\text{A7})$$

833 We thus suggest  $\tau = RC/10$  as a convenient rule of thumb for the timescale at  
 834 which a lightning channel becomes an equipotential. Strictly speaking this approxima-  
 835 tion is only valid for a stationary channel which suddenly develops in a uniform field,  
 836 but it may still be a useful reference for a more realistic model of leader development.

## 837 Appendix B Open Research

838 The 3D mapping and field change data used for this paper has previously been made  
 839 available online (Jensen et al., 2023a). All data files are in text format with headers that  
 840 describe each data column. A PDF is included which describes the included files, and  
 841 gives examples of the headers and column format.

## 842 Acknowledgments

843 We would like to acknowledge an undergraduate student paper written by Qianui Qi of  
 844 the Pennsylvania State University: Department of Electrical Engineering for providing  
 845 the initial framework for the equipotential model calculations, as an adapted form of the  
 846 methods reported by Mazur and Ruhnke (1998). We would also like to thank Steve Cum-  
 847 mer for suggesting that we explicitly model the branch junction interaction when an early  
 848 version of this work was presented at the AGU 2023 Fall Meeting.

849 Research presented in this article was supported by the Laboratory Directed Re-  
 850 search and Development program of Los Alamos National Laboratory under project num-  
 851 ber 20230223ER, and the Los Alamos National Laboratory Center for Space and Envi-  
 852 ronmental Science under project number [-enter project number-]. Additional funding for  
 853 this work was provided by the New Mexico Consortium under #Subcontract No: 038508  
 854 to New Mexico Tech.

## 855 References

- 856 Andreev, A., Bazelyan, E., Bulatov, M., Kuzhekin, I., Makalsky, L., Sukharevskij,  
 857 D., & Syssoev, V. (2008). Experimental study of the positive leader ve-  
 858 locity as a function of the current in the initial and final-jump phases of  
 859 a spark discharge. *Plasma Physics Reports*, *34*, 609–615. Retrieved from  
 860 <https://doi.org/10.1134/S1063780X0807009X>
- 861 Babaeva, N., & Naidis, G. (1997). Dynamics of positive and negative streamers  
 862 in air in weak uniform electric fields. *IEEE Transactions on Plasma Science*,  
 863 *25*(2), 375–379. doi: 10.1109/27.602514
- 864 Bazelyan, E. M., & Raizer, Y. P. (1997). *Spark discharge*. CRC press.
- 865 Bazelyan, E. M., & Raizer, Y. P. (2000). *Lightning physics and lightning protection*.  
 866 CRC Press.
- 867 Briels, T. M. P., Kos, J., Winands, G. J. J., van Veldhuizen, E. M., & Ebert, U.  
 868 (2008, nov). Positive and negative streamers in ambient air: measuring diam-  
 869 eter, velocity and dissipated energy. *Journal of Physics D: Applied Physics*,

- 870 41(23), 234004. Retrieved from [https://dx.doi.org/10.1088/0022-3727/](https://dx.doi.org/10.1088/0022-3727/41/23/234004)  
871 41/23/234004 doi: 10.1088/0022-3727/41/23/234004
- 872 Cai, L., Chu, W., Wang, J., Zhou, M., Yan, Y., Tian, R., & Fan, Y. (2022). Ob-  
873 servation and modeling of dart leader development in an altitude-triggered  
874 lightning flash. *Journal of Geophysical Research: Atmospheres*, 127(24),  
875 e2022JD037545. Retrieved from [https://agupubs.onlinelibrary.wiley](https://agupubs.onlinelibrary.wiley.com/doi/abs/10.1029/2022JD037545)  
876 [.com/doi/abs/10.1029/2022JD037545](https://doi.org/10.1029/2022JD037545) (e2022JD037545 2022JD037545) doi:  
877 <https://doi.org/10.1029/2022JD037545>
- 878 Celestin, S., & Pasko, V. P. (2011). Energy and fluxes of thermal runaway elec-  
879 trons produced by exponential growth of streamers during the stepping  
880 of lightning leaders and in transient luminous events. *Journal of Geo-*  
881 *physical Research: Space Physics*, 116(A3). Retrieved from [https://](https://agupubs.onlinelibrary.wiley.com/doi/abs/10.1029/2010JA016260)  
882 [agupubs.onlinelibrary.wiley.com/doi/abs/10.1029/2010JA016260](https://doi.org/10.1029/2010JA016260) doi:  
883 <https://doi.org/10.1029/2010JA016260>
- 884 Chang, X., Yuan, P., Cen, J., & Wang, X. (2017). Variation of the channel  
885 temperature in the transmission of lightning leader. *Journal of Atmo-*  
886 *spheric and Solar-Terrestrial Physics*, 159, 41-47. Retrieved from [https://](https://www.sciencedirect.com/science/article/pii/S1364682617300123)  
887 [www.sciencedirect.com/science/article/pii/S1364682617300123](https://doi.org/10.1016/j.jastp.2017.04.006) doi:  
888 <https://doi.org/10.1016/j.jastp.2017.04.006>
- 889 Chen, M., Zheng, D., Du, Y., & Zhang, Y. (2013). Evolution of line charge density  
890 of steadily-developing upward positive leaders in triggered lightning. *Journal*  
891 *of Geophysical Research: Atmospheres*, 118(10), 4670-4678. Retrieved from  
892 <https://agupubs.onlinelibrary.wiley.com/doi/abs/10.1002/jgrd.50446>  
893 doi: <https://doi.org/10.1002/jgrd.50446>
- 894 Cooray, V., Becerra, M., & Rakov, V. (2009). On the electric field at the  
895 tip of dart leaders in lightning flashes. *Journal of Atmospheric and*  
896 *Solar-Terrestrial Physics*, 71(12), 1397-1404. Retrieved from [https://](https://www.sciencedirect.com/science/article/pii/S1364682609001497)  
897 [www.sciencedirect.com/science/article/pii/S1364682609001497](https://doi.org/10.1016/j.jastp.2009.06.002) doi:  
898 <https://doi.org/10.1016/j.jastp.2009.06.002>
- 899 Cummer, S. A. (2020). Indirectly measured ambient electric fields for light-  
900 ning initiation in fast breakdown regions. *Geophysical Research Letters*,  
901 47(4), e2019GL086089. Retrieved from [https://agupubs.onlinelibrary](https://agupubs.onlinelibrary.wiley.com/doi/abs/10.1029/2019GL086089)  
902 [.wiley.com/doi/abs/10.1029/2019GL086089](https://doi.org/10.1029/2019GL086089) (e2019GL086089  
903 10.1029/2019GL086089) doi: <https://doi.org/10.1029/2019GL086089>
- 904 da Silva, C. L., & Pasko, V. P. (2013). Dynamics of streamer-to-leader transi-  
905 tion at reduced air densities and its implications for propagation of lightning  
906 leaders and gigantic jets. *Journal of Geophysical Research: Atmospheres*,  
907 118(24), 13,561-13,590. Retrieved from [https://agupubs.onlinelibrary](https://agupubs.onlinelibrary.wiley.com/doi/abs/10.1002/2013JD020618)  
908 [.wiley.com/doi/abs/10.1002/2013JD020618](https://doi.org/10.1002/2013JD020618) doi: [https://doi.org/10.1002/](https://doi.org/10.1002/2013JD020618)  
909 [2013JD020618](https://doi.org/10.1002/2013JD020618)
- 910 da Silva, C. L., & Pasko, V. P. (2015). Physical mechanism of initial breakdown  
911 pulses and narrow bipolar events in lightning discharges. *Journal of Geophys-*  
912 *ical Research: Atmospheres*, 120(10), 4989-5009. Retrieved from [https://](https://agupubs.onlinelibrary.wiley.com/doi/abs/10.1002/2015JD023209)  
913 [agupubs.onlinelibrary.wiley.com/doi/abs/10.1002/2015JD023209](https://doi.org/10.1002/2015JD023209) doi:  
914 <https://doi.org/10.1002/2015JD023209>
- 915 da Silva, C. L., Sonnenfeld, R. G., Edens, H. E., Krehbiel, P. R., Quick, M. G., &  
916 Koshak, W. J. (2019). The plasma nature of lightning channels and the result-  
917 ing nonlinear resistance. *Journal of Geophysical Research: Atmospheres*,  
918 124(16), 9442-9463. Retrieved from [https://agupubs.onlinelibrary](https://agupubs.onlinelibrary.wiley.com/doi/abs/10.1029/2019JD030693)  
919 [.wiley.com/doi/abs/10.1029/2019JD030693](https://doi.org/10.1029/2019JD030693) doi: [https://doi.org/10.1029/](https://doi.org/10.1029/2019JD030693)  
920 [2019JD030693](https://doi.org/10.1029/2019JD030693)
- 921 da Silva, C. L., Winn, W. P., Taylor, M. C., Aulich, G. D., Hunyady, S. J., Eack,  
922 K. B., ... Trueblood, J. J. (2023). Polarity asymmetries in rocket-triggered  
923 lightning. *Geophysical Research Letters*, 50(17), e2023GL105041. Retrieved  
924 from <https://agupubs.onlinelibrary.wiley.com/doi/abs/10.1029/>

- 2023GL105041 (e2023GL105041 2023GL105041) doi: <https://doi.org/10.1029/2023GL105041>
- Ding, Z., Rakov, V. A., Zhu, Y., Kereszy, I., Chen, S., & Tran, M. D. (2024). Propagation mechanism of branched downward positive leader resulting in a negative cloud-to-ground flash. *Journal of Geophysical Research: Atmospheres*, *129*(1), e2023JD039262. Retrieved from <https://agupubs.onlinelibrary.wiley.com/doi/abs/10.1029/2023JD039262> (e2023JD039262 2023JD039262) doi: <https://doi.org/10.1029/2023JD039262>
- Edens, H. E., Eack, K. B., Rison, W., & Hunyady, S. J. (2014). Photographic observations of streamers and steps in a cloud-to-air negative leader. *Geophysical Research Letters*, *41*(4), 1336-1342. Retrieved from <https://agupubs.onlinelibrary.wiley.com/doi/abs/10.1002/2013GL059180> doi: <https://doi.org/10.1002/2013GL059180>
- Födösch, P., Wohsmann, J., Lange, B., Schönherr, J., Enghardt, W., & Kaever, P. (2016). Digital high-pass filter deconvolution by means of an infinite impulse response filter. *Nuclear Instruments and Methods in Physics Research Section A: Accelerators, Spectrometers, Detectors and Associated Equipment*, *830*, 484-496. Retrieved from <https://www.sciencedirect.com/science/article/pii/S0168900216305617> doi: <https://doi.org/10.1016/j.nima.2016.06.019>
- Gao, Y., Chen, M., Lyu, W., Qi, Q., Qin, Z., Du, Y.-p., & Zhang, Y. (2020). Leader charges, currents, ambient electric fields, and space charges along downward positive leader paths retrieved from ground measurements in metropolis. *Journal of Geophysical Research: Atmospheres*, *125*(19), e2020JD032818. Retrieved from <https://agupubs.onlinelibrary.wiley.com/doi/abs/10.1029/2020JD032818> (e2020JD032818 2020JD032818) doi: <https://doi.org/10.1029/2020JD032818>
- Hare, B. M., Scholten, O., Buitink, S., Dwyer, J., Liu, N., Sterpka, C., & Veen, S. T. (2023b). Vhf emitting width and 3d polarization of lightning dart leaders. In *2023 xxvth general assembly and scientific symposium of the international union of radio science (ursi gass)* (p. 1-4). doi: 10.23919/URSIGASS57860.2023.10265623
- Hare, B. M., Scholten, O., Buitink, S., Dwyer, J. R., Liu, N., Sterpka, C., & ter Veen, S. (2023a, Jan). Characteristics of recoil leaders as observed by lofar. *Phys. Rev. D*, *107*, 023025. Retrieved from <https://link.aps.org/doi/10.1103/PhysRevD.107.023025> doi: 10.1103/PhysRevD.107.023025
- Hare, B. M., Scholten, O., Ľureková, P., Cummer, S., Dwyer, J., Liu, N., ... ter Veen, S. (2024, April). Lofar observations of the initial stage of ic dart leaders. In *Egu general assembly 2024* (p. EGU24-7940). Vienna, Austria. doi: <https://doi.org/10.5194/egusphere-egu24-7940>
- Jackson, J. D. (2000, 09). Charge density on thin straight wire, revisited. *American Journal of Physics*, *68*(9), 789-799. Retrieved from <https://doi.org/10.1119/1.1302908> doi: 10.1119/1.1302908
- Jensen, D. P., Shao, X.-M., & Sonnenfeld, R. (2023a). *Data and Supplementary Material for "Insights into Lightning K-Leader Initiation and Development from Three Dimensional Broadband Interferometric Observations" by Jensen et al.* Zenodo. Retrieved from <https://doi.org/10.5281/zenodo.8213032> ([Dataset]) doi: 10.5281/zenodo.8213032
- Jensen, D. P., Shao, X.-M., & Sonnenfeld, R. G. (2023b). Insights into lightning k-leader initiation and development from three dimensional broadband interferometric observations. *Journal of Geophysical Research: Atmospheres*, *128*(23), e2023JD039104. Retrieved from <https://agupubs.onlinelibrary.wiley.com/doi/abs/10.1029/2023JD039104> (e2023JD039104 2023JD039104) doi: <https://doi.org/10.1029/2023JD039104>
- Jensen, D. P., Sonnenfeld, R. G., Stanley, M. A., Edens, H. E., da Silva, C. L., & Krehbiel, P. R. (2021). Dart-leader and k-leader velocity from initiation

- 980 site to termination time-resolved with 3d interferometry. *Journal of Geo-*  
 981 *physical Research: Atmospheres*, e2020JD034309. Retrieved from [https://](https://agupubs.onlinelibrary.wiley.com/doi/abs/10.1029/2020JD034309)  
 982 [agupubs.onlinelibrary.wiley.com/doi/abs/10.1029/2020JD034309](https://agupubs.onlinelibrary.wiley.com/doi/abs/10.1029/2020JD034309) doi:  
 983 <https://doi.org/10.1029/2020JD034309>
- 984 Karunarathne, S., Marshall, T. C., Stolzenburg, M., Karunarathna, N., & Orville,  
 985 R. E. (2015). Modeling stepped leaders using a time-dependent mul-  
 986 tidipole model and high-speed video data. *Journal of Geophysical Re-*  
 987 *search: Atmospheres*, 120(6), 2419-2436. Retrieved from [https://](https://agupubs.onlinelibrary.wiley.com/doi/abs/10.1002/2014JD022679)  
 988 [agupubs.onlinelibrary.wiley.com/doi/abs/10.1002/2014JD022679](https://agupubs.onlinelibrary.wiley.com/doi/abs/10.1002/2014JD022679) doi:  
 989 <https://doi.org/10.1002/2014JD022679>
- 990 Kasemir, H. W. (1960). A contribution to the electrostatic theory of a lightning  
 991 discharge. *Journal of Geophysical Research (1896-1977)*, 65(7), 1873-1878.  
 992 Retrieved from [https://agupubs.onlinelibrary.wiley.com/doi/abs/](https://agupubs.onlinelibrary.wiley.com/doi/abs/10.1029/JZ065i007p01873)  
 993 [10.1029/JZ065i007p01873](https://agupubs.onlinelibrary.wiley.com/doi/abs/10.1029/JZ065i007p01873) doi: <https://doi.org/10.1029/JZ065i007p01873>
- 994 King, L. (1962). The voltage gradient of the free burning arc in air or nitrogen. *Ion-*  
 995 *ization Phenomena in Gases, Volume I*, 871.
- 996 Lu, G., Winn, W. P., & Sonnenfeld, R. G. (2011). Charge transfer during in-  
 997 tracloud lightning from a time-dependent multidipole model. *Journal of*  
 998 *Geophysical Research: Atmospheres*, 116(D3). Retrieved from [https://](https://agupubs.onlinelibrary.wiley.com/doi/abs/10.1029/2010JD014495)  
 999 [agupubs.onlinelibrary.wiley.com/doi/abs/10.1029/2010JD014495](https://agupubs.onlinelibrary.wiley.com/doi/abs/10.1029/2010JD014495) doi:  
 1000 <https://doi.org/10.1029/2010JD014495>
- 1001 Marshall, T. C., Stolzenburg, M., Rust, W. D., Williams, E. R., & Boldi, R. (2001).  
 1002 Positive charge in the stratiform cloud of a mesoscale convective system. *Jour-*  
 1003 *nal of Geophysical Research: Atmospheres*, 106(D1), 1157-1163. Retrieved  
 1004 from [https://agupubs.onlinelibrary.wiley.com/doi/abs/10.1029/](https://agupubs.onlinelibrary.wiley.com/doi/abs/10.1029/2000JD900625)  
 1005 [2000JD900625](https://agupubs.onlinelibrary.wiley.com/doi/abs/10.1029/2000JD900625) doi: <https://doi.org/10.1029/2000JD900625>
- 1006 Mazur, V. (2016). The physical concept of recoil leader formation. *Journal of*  
 1007 *Electrostatics*, 82, 79–87. Retrieved from [https://www.sciencedirect.com/](https://www.sciencedirect.com/science/article/pii/S0304388616300407)  
 1008 [science/article/pii/S0304388616300407](https://www.sciencedirect.com/science/article/pii/S0304388616300407) doi: [https://doi.org/10.1016/](https://doi.org/10.1016/j.elstat.2016.05.005)  
 1009 [j.elstat.2016.05.005](https://doi.org/10.1016/j.elstat.2016.05.005)
- 1010 Mazur, V., & Ruhnke, L. H. (1993). Common physical processes in nat-  
 1011 ural and artificially triggered lightning. *Journal of Geophysical Re-*  
 1012 *search: Atmospheres*, 98(D7), 12913-12930. Retrieved from [https://](https://agupubs.onlinelibrary.wiley.com/doi/abs/10.1029/93JD00626)  
 1013 [agupubs.onlinelibrary.wiley.com/doi/abs/10.1029/93JD00626](https://agupubs.onlinelibrary.wiley.com/doi/abs/10.1029/93JD00626) doi:  
 1014 <https://doi.org/10.1029/93JD00626>
- 1015 Mazur, V., & Ruhnke, L. H. (1998). Model of electric charges in thunderstorms and  
 1016 associated lightning. *Journal of Geophysical Research: Atmospheres*, 103(D18),  
 1017 23299-23308. Retrieved from [https://agupubs.onlinelibrary.wiley.com/](https://agupubs.onlinelibrary.wiley.com/doi/abs/10.1029/98JD02120)  
 1018 [doi/abs/10.1029/98JD02120](https://agupubs.onlinelibrary.wiley.com/doi/abs/10.1029/98JD02120) doi: <https://doi.org/10.1029/98JD02120>
- 1019 Mazur, V., & Ruhnke, L. H. (2014). The physical processes of current cutoff in  
 1020 lightning leaders. *Journal of Geophysical Research: Atmospheres*, 119(6),  
 1021 2796–2810.
- 1022 Mazur, V., Ruhnke, L. H., & Laroche, P. (1995). The relationship of leader  
 1023 and return stroke processes in cloud-to-ground lightning. *Geophys-*  
 1024 *ical Research Letters*, 22(19), 2613-2616. Retrieved from [https://](https://agupubs.onlinelibrary.wiley.com/doi/abs/10.1029/95GL02348)  
 1025 [agupubs.onlinelibrary.wiley.com/doi/abs/10.1029/95GL02348](https://agupubs.onlinelibrary.wiley.com/doi/abs/10.1029/95GL02348) doi:  
 1026 <https://doi.org/10.1029/95GL02348>
- 1027 Miki, M., Rakov, V. A., Rambo, K. J., Schnetzer, G. H., & Uman, M. A. (2002).  
 1028 Electric fields near triggered lightning channels measured with pockels sensors.  
 1029 *Journal of Geophysical Research: Atmospheres*, 107(D16), ACL 2-1-ACL 2-  
 1030 11. Retrieved from [https://agupubs.onlinelibrary.wiley.com/doi/abs/](https://agupubs.onlinelibrary.wiley.com/doi/abs/10.1029/2001JD001087)  
 1031 [10.1029/2001JD001087](https://agupubs.onlinelibrary.wiley.com/doi/abs/10.1029/2001JD001087) doi: <https://doi.org/10.1029/2001JD001087>
- 1032 Montano, R., Becerra, M., Cooray, V., Rahman, M., & Liyanage, P. (2006). Resis-  
 1033 tance of spark channels. *IEEE Transactions on Plasma Science*, 34(5), 1610-  
 1034 1619. doi: 10.1109/TPS.2006.883350

- 1035 Nag, A., Rakov, V. A., & Cummins, K. L. (2014). Positive lightning peak currents  
1036 reported by the u.s. national lightning detection network. *IEEE Transactions*  
1037 *on Electromagnetic Compatibility*, *56*(2), 404-412. doi: 10.1109/TEMC.2013  
1038 .2280000
- 1039 Orville, R. E. (1975). Spectrum of the lightning dart leader. *Journal of Atmospheric*  
1040 *Sciences*, *32*(9), 1829 - 1837. Retrieved from [https://journals.ametsoc](https://journals.ametsoc.org/view/journals/atsc/32/9/1520-0469_1975_032_1829_sot1d1_2_0_co_2.xml)  
1041 [.org/view/journals/atsc/32/9/1520-0469\\_1975\\_032\\_1829\\_sot1d1\\_2\\_0\\_co\\_2](https://journals.ametsoc.org/view/journals/atsc/32/9/1520-0469_1975_032_1829_sot1d1_2_0_co_2.xml)  
1042 [.xml](https://journals.ametsoc.org/view/journals/atsc/32/9/1520-0469_1975_032_1829_sot1d1_2_0_co_2.xml) doi: 10.1175/1520-0469(1975)032<1829:SOTLDL>2.0.CO;2
- 1043 Pasko, V. P. (2014). Electrostatic modeling of intracloud stepped leader  
1044 electric fields and mechanisms of terrestrial gamma ray flashes. *Geo-*  
1045 *physical Research Letters*, *41*(1), 179-185. Retrieved from [https://](https://agupubs.onlinelibrary.wiley.com/doi/abs/10.1002/2013GL058983)  
1046 [agupubs.onlinelibrary.wiley.com/doi/abs/10.1002/2013GL058983](https://agupubs.onlinelibrary.wiley.com/doi/abs/10.1002/2013GL058983) doi:  
1047 <https://doi.org/10.1002/2013GL058983>
- 1048 Petersen, D. A., & Beasley, W. H. (2013). High-speed video observations of a nat-  
1049 ural negative stepped leader and subsequent dart-stepped leader. *Journal*  
1050 *of Geophysical Research: Atmospheres*, *118*(21), 12,110-12,119. Retrieved  
1051 from [https://agupubs.onlinelibrary.wiley.com/doi/abs/10.1002/](https://agupubs.onlinelibrary.wiley.com/doi/abs/10.1002/2013JD019910)  
1052 [2013JD019910](https://agupubs.onlinelibrary.wiley.com/doi/abs/10.1002/2013JD019910) doi: <https://doi.org/10.1002/2013JD019910>
- 1053 Qin, J., & Pasko, V. P. (2014, oct). On the propagation of streamers in electrical  
1054 discharges. *Journal of Physics D: Applied Physics*, *47*(43), 435202. Retrieved  
1055 from <https://dx.doi.org/10.1088/0022-3727/47/43/435202> doi: 10.1088/  
1056 [0022-3727/47/43/435202](https://dx.doi.org/10.1088/0022-3727/47/43/435202)
- 1057 Rakov, V. A. (1998). Some inferences on the propagation mechanisms of dart leaders  
1058 and return strokes. *Journal of Geophysical Research: Atmospheres*, *103*(D2),  
1059 1879-1887. Retrieved from [https://agupubs.onlinelibrary.wiley.com/](https://agupubs.onlinelibrary.wiley.com/doi/abs/10.1029/97JD03116)  
1060 [doi/abs/10.1029/97JD03116](https://agupubs.onlinelibrary.wiley.com/doi/abs/10.1029/97JD03116) doi: 10.1029/97JD03116
- 1061 Rakov, V. A., Thottappillil, R., & Uman, M. A. (1992). On the empirical formula  
1062 of willett et al. relating lightning return-stroke peak current and peak electric  
1063 field. *Journal of Geophysical Research: Atmospheres*, *97*(D11), 11527-11533.  
1064 Retrieved from [https://agupubs.onlinelibrary.wiley.com/doi/abs/](https://agupubs.onlinelibrary.wiley.com/doi/abs/10.1029/92JD00720)  
1065 [10.1029/92JD00720](https://agupubs.onlinelibrary.wiley.com/doi/abs/10.1029/92JD00720) doi: <https://doi.org/10.1029/92JD00720>
- 1066 Rakov, V. A., & Uman, M. A. (2003). *Lightning: physics and effects*. Cambridge  
1067 university press.
- 1068 Shao, X.-M., Jensen, D., Ho, C., Graham, P., Haynes, W., Caffrey, M., ... Sonnen-  
1069 feld, R. (2023). Three-dimensional broadband interferometric mapping and  
1070 polarization (bimap-3d) observations of lightning discharge processes. *Journal*  
1071 *of Geophysical Research: Atmospheres*, *128*(4), e2022JD037955. Retrieved  
1072 from [https://agupubs.onlinelibrary.wiley.com/doi/abs/10.1029/](https://agupubs.onlinelibrary.wiley.com/doi/abs/10.1029/2022JD037955)  
1073 [2022JD037955](https://agupubs.onlinelibrary.wiley.com/doi/abs/10.1029/2022JD037955) (e2022JD037955 2022JD037955) doi: [https://doi.org/10.1029/](https://doi.org/10.1029/2022JD037955)  
1074 [2022JD037955](https://doi.org/10.1029/2022JD037955)
- 1075 Sonnenfeld, R. G., Battles, J. D., Lu, G., & Winn, W. P. (2006). Compar-  
1076 ing e field changes aloft to lightning mapping data. *Journal of Geo-*  
1077 *physical Research: Atmospheres*, *111*(D20). Retrieved from [https://](https://agupubs.onlinelibrary.wiley.com/doi/abs/10.1029/2006JD007242)  
1078 [agupubs.onlinelibrary.wiley.com/doi/abs/10.1029/2006JD007242](https://agupubs.onlinelibrary.wiley.com/doi/abs/10.1029/2006JD007242) doi:  
1079 <https://doi.org/10.1029/2006JD007242>
- 1080 Sonnenfeld, R. G., Jensen, D. P., Contreras-Vidal, L., Pantuso, J., daSilva, C. L.,  
1081 Clonch, C., ... Edens, H. E. (2023). Detailed streamer observations & model-  
1082 ing of a nearby negative flash. *Authorea Preprints*. Retrieved from [https://](https://essopenarchive.org/doi/full/10.22541/essoar.170240442.22551037)  
1083 [essopenarchive.org/doi/full/10.22541/essoar.170240442.22551037](https://essopenarchive.org/doi/full/10.22541/essoar.170240442.22551037)
- 1084 Stolzenburg, M., & Marshall, T. C. (2008). Charge structure and dynamics in thun-  
1085 derstorms. *Space Science Reviews*, *137*, 355-372. doi: [https://doi.org/10.1007/](https://doi.org/10.1007/s11214-008-9338-z)  
1086 [s11214-008-9338-z](https://doi.org/10.1007/s11214-008-9338-z)
- 1087 Stolzenburg, M., Marshall, T. C., Karunarathne, S., Karunarathna, N., & Orville,  
1088 R. E. (2015). Transient luminosity along negative stepped leaders in light-  
1089 ning. *Journal of Geophysical Research: Atmospheres*, *120*(8), 3408-3435.

- 1090 Retrieved from [https://agupubs.onlinelibrary.wiley.com/doi/abs/](https://agupubs.onlinelibrary.wiley.com/doi/abs/10.1002/2014JD022933)  
1091 10.1002/2014JD022933 doi: <https://doi.org/10.1002/2014JD022933>
- 1092 Stolzenburg, M., Marshall, T. C., Rust, W. D., Bruning, E., MacGorman, D. R.,  
1093 & Hamlin, T. (2007). Electric field values observed near lightning flash ini-  
1094 tiations. *Geophysical Research Letters*, 34(4). Retrieved from [https://](https://agupubs.onlinelibrary.wiley.com/doi/abs/10.1029/2006GL028777)  
1095 [agupubs.onlinelibrary.wiley.com/doi/abs/10.1029/2006GL028777](https://agupubs.onlinelibrary.wiley.com/doi/abs/10.1029/2006GL028777) doi:  
1096 <https://doi.org/10.1029/2006GL028777>
- 1097 Uman, M. A., & Voshall, R. E. (1968). Time interval between lightning strokes and  
1098 the initiation of dart leaders. *Journal of Geophysical Research (1896-1977)*,  
1099 73(2), 497-506. Retrieved from [https://agupubs.onlinelibrary.wiley](https://agupubs.onlinelibrary.wiley.com/doi/abs/10.1029/JB073i002p00497)  
1100 [.com/doi/abs/10.1029/JB073i002p00497](https://agupubs.onlinelibrary.wiley.com/doi/abs/10.1029/JB073i002p00497) doi: [JB073i002p00497](https://doi.org/10.1029/</a><br/>1101 <a href=)
- 1102 Willett, J. C., Bailey, J. C., Idone, V. P., Eybert-Berard, A., & Barret, L. (1989).  
1103 Submicrosecond intercomparison of radiation fields and currents in triggered  
1104 lightning return strokes based on the transmission-line model. *Journal of*  
1105 *Geophysical Research: Atmospheres*, 94(D11), 13275-13286. Retrieved  
1106 from [https://agupubs.onlinelibrary.wiley.com/doi/abs/10.1029/](https://agupubs.onlinelibrary.wiley.com/doi/abs/10.1029/JD094iD11p13275)  
1107 [JD094iD11p13275](https://agupubs.onlinelibrary.wiley.com/doi/abs/10.1029/JD094iD11p13275) doi: <https://doi.org/10.1029/JD094iD11p13275>
- 1108 Yos, J. M. (1963). *Transport properities of nitrogen, hydrogen, oxygen, and air to*  
1109 *30,000 k*. Clearinghouse for Federal Scientific and Technical Information.